Mobility Gradients Yield Rubbery Surfaces atop Polymer Glasses

Zhiwei Hao^{1,†}, Asieh Ghanekarade^{2,†}, Ningtao Zhu¹, Katelyn Randazzo³, Daisuke Kawaguchi⁵, Keiji Tanaka^{5,6}, Xinping Wang¹, David S. Simmons^{2,*}, Rodney D. Priestley^{3,4,*}, and Biao Zuo^{1,*}

Affiliations:

- Department of Chemistry, Key Laboratory of Surface & Interface Science of Polymer Materials of Zhejiang Province, National Engineering Lab for Textile Fiber Materials and Processing Technology (Zhejiang), Zhejiang Sci-Tech University, Hangzhou, China.
 - ² Department of Chemical and Biomedical Engineering, University of South Florida, Tampa, Florida, United States.
- Department of Chemical and Biological Engineering, Princeton University, Princeton, New Jersey, United States.
 - ⁴ Princeton Institute for the Science and Technology of Materials, Princeton University, Princeton, New Jersey, United States.
 - ⁵ Department of Applied Chemistry, Center for Polymer Interface and Molecular Adhesion Science, Kyushu University, Fukuoka, Japan.
 - ⁶ International Institute for Carbon-Neutral Energy Research (WPI-I2CNER), Kyushu University, Fukuoka, Japan.
 - *Correspondence to: dssimmons@usf.edu (for DSS); rpriestl@princeton.edu (for RDP) chemizuo@zstu.edu.cn (for BZ)

15

[†]These authors contributed equally to this work.

Summary Paragraph: The discovery of enormous changes in dynamics near interfaces in glass-forming liquids ^{1 - 3} has reshaped the understanding of nanoscale materials' behavior and revolutionized the use of interfaces to enable new materials, such as ultra-stable glasses ^{4,5} with extraordinary properties. In polymers, the nature of these interfacial modifications is even more complex due to a second length scale – the chain size – that exists in parallel to the length scale of interfacial gradients in segmental dynamics ⁶⁻⁹. Here, *via* simulations and time-resolved surface nano-creep experiments, we reveal the implications of this two-scale nature of glassy polymer surfaces: it drives the emergence of a transient rubbery, entangled-like surface behavior even in short, subentangled chains. A proposed mean-field theory demonstrates that this effect emerges from superposed gradients in segmental dynamics and chain conformational statistics. The lifetime of this behavior grows on cooling, leading to a general surface breakdown in time-temperature-superposition (TTS) – a fundamental tenet of polymer physics and rheology. This discovery has broad implications, indicating that this interfacial transient elastomer effect and TTS breakdown should be the norm in the wide range of macromolecular systems, from nanocomposites to thin films, in which interfaces dominate these materials^{3,10}.

Main Text: The discovery in the early 1990s that the glass transition temperature (T_g) of molecular 11 and polymeric 12 glass formers can deviate enormously from the bulk under nanoconfinement and near interfaces has since been the subject of immense study. We now know that the surface of many glasses is not glassy $^{1-10}$. Rather, at the surface of glassy materials there exists a surface mobile layer typically of order 10 nm in thickness, wherein molecular mobility is exceedingly faster than in the bulk $^{13-17}$. This domain of fast surface dynamics, which corresponds to a smooth exponential gradient of $T_g^{6-9,18}$, has major implications for material properties. For example, in ultrathin films, this near-surface domain is now recognized as the cause for deviations in $T_g^{3,12,16}$, as well as other important properties including viscosity 16 , physical aging 9 , diffusion 19 , thermal expansivity 12,20 and crystallization 10 . The formation of ultrastable glasses is also enabled by this layer of enhanced surface dynamics 4,5 . Enhanced surface dynamics can further account for tribological and adhesive properties $^{21-23}$ that allow for cold joining 24 and low-temperature processing of glassy materials 25 . Unveiling the mechanisms underlying the surface dynamics of glasses would thus enhance our ability to exploit interfaces to tune material properties.

This situation is more complex for polymers, the dynamics of which involve motion across multiple molecular length scales: segmental motions build up to Rouse relaxations of strands, up to the length scale of topological entanglements between chains, which give way to snakelike reptation motions mediating diffusion at the longest chain scales. Because these length scales can be comparable to or greater than the range of the surface mobile region, a recent perspective pointed out that "It remains unknown whether surface diffusion is possible for long-chain

polymers²⁶. Understanding the fundamental nature of near-surface polymer motion thus remains a challenge. Moreover, whereas classical viscoelastic theories predict shared temperature dependences and TTS across all of these chain modes, ²⁷ it is known that bulk dynamic heterogeneity can cause a breakdown of thermorheological simplicity near $T_g^{28,29}$. This thus raises a related question: *How do interfaces modify the temperature dependence of polymer chain motion*?

Here we employ a nanoscale surface creep experiment, driven by interfacial wetting over an immiscible liquid droplet on a polymer surface, to reveal the nature of polymer chain motion at surfaces. As shown in Fig. 1a, in this geometry the normal interfacial force acting in the microscopic region of the three-phase line draws the polymer surface up to form a well-defined wetting ridge³⁰⁻³², the height (d) of which is determined by balanced contributions from the vertical force and material compliance (D), *i.e.*, $d \sim D \cdot \gamma_l \sin\theta^{30-32}$. The evolution of d with droplet placement time (t) thus reflects the relaxation of the surface creep of the polymer, *i.e.*, $D_t \sim d_t \sim t$, revealing polymer surface mechanics; see Methods for procedural details. The forming stress (σ) due to the surface tension, ($\sigma \approx \gamma_l \sin\theta/w^{30,31}$; w is width of the ridge, generally larger than 10 nm) is smaller than the yield stress of PS, indicating a linear viscoelastic response.

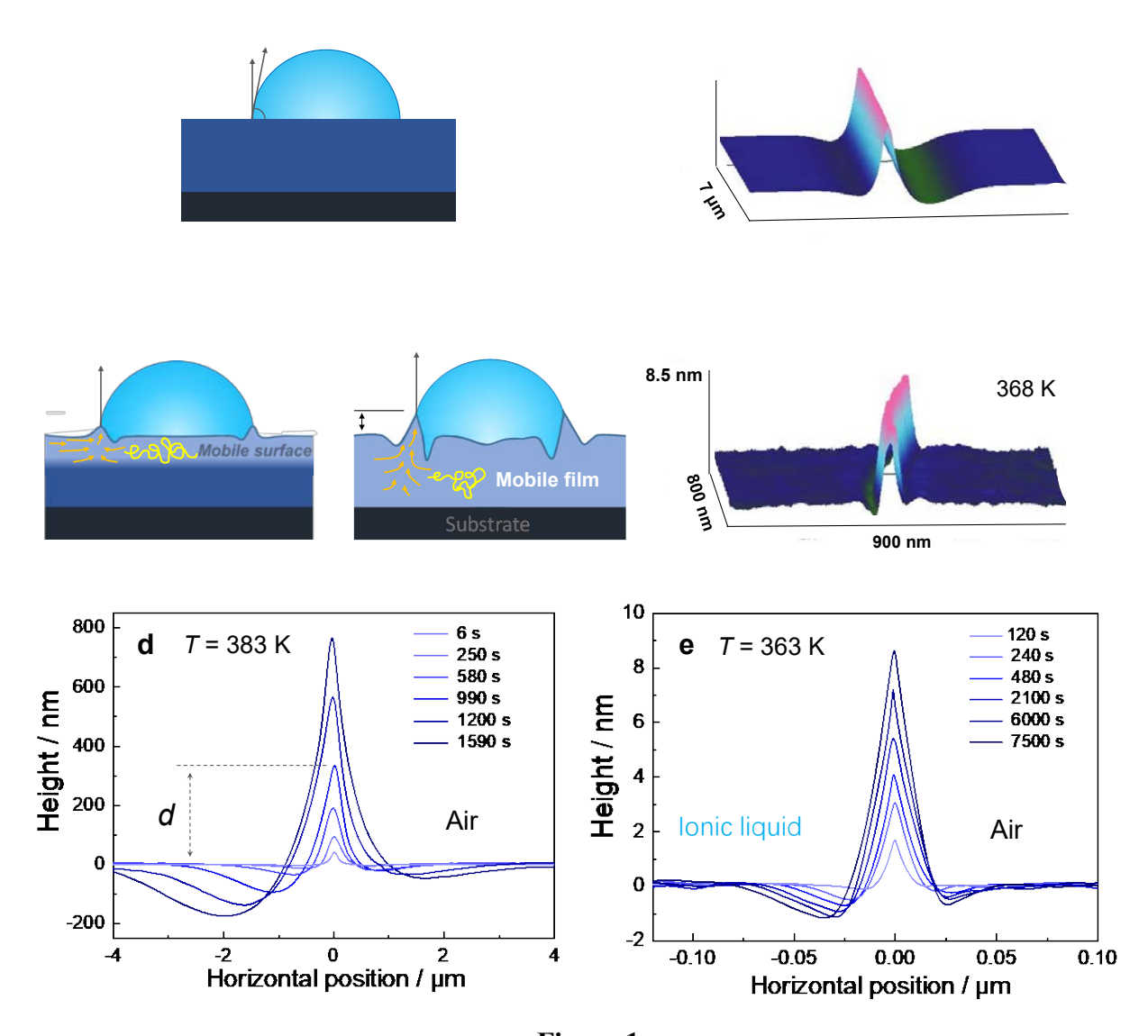


Figure 1

We perform the experiment on polystyrene (PS) films with a 1-ethyl-3-methylimidazolium tetrafluoroborate ([EIm]BF4) droplet; as shown in Tab. S1 and Figs. S1-S4 in the Supplementary information (SI), this pairing provides good stability and avoids swelling or plasticization effects³³. We focus initially on an entangled PS of molecular weight (M_w) 52 kg/mol $-\sim 4$ times the entanglement molecular weight M_e of PS $(13 \text{ kg/mol})^{34}$ with a polydispersity index of 1.06 and a bulk T_g ($T_{g,\text{bulk}}$) equal to 374 K. The PS chain unperturbed gyration radius (R_g) is approximately 6.2 nm. Given the evidence a similar order-of-magnitude of length scale in the gradient of enhanced surface dynamics^{7,9,19}, each chain at the surface is expected to sample a range of local interfacial dynamics within the surface gradient.

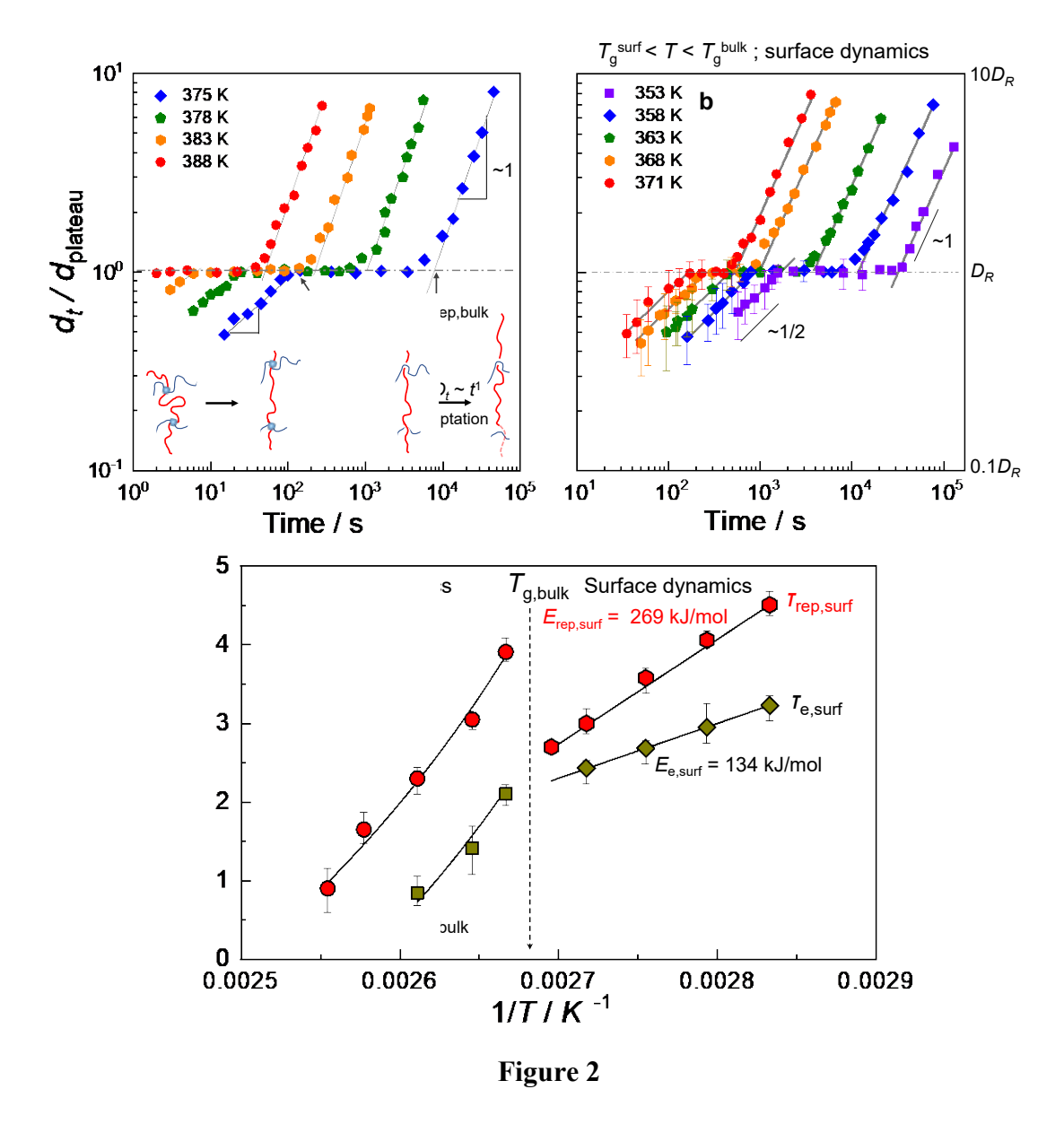
5

10

As illustrated by AFM topological traces at 380 K ($T_{\rm g,bulk}$ + 6 K) in Fig. 1b, at high temperatures the entire film flows to produce large deformations (*i.e.*, $d \sim 320$ nm). In contrast,

results at 368 K ($T_{g,bulk}$ - 6 K) illustrate that, below T_g , only the surface layer remains mobile, producing a small wetting ridge with $d \sim 8$ nm (see Fig. 1c). As shown in Fig. S5 in the SI, an associated sharp drop in d as the temperature drops through $T_{g,bulk}$ indicates a transition from bulk flow at $T > T_{g,bulk}$ to surface dominated flow at $T < T_{g,bulk}$. Figs. 1 d and e show the progressive increment of d with time due to bulk and surface flow, respectively.

As shown in Figs. 2 a and b, the time evolution of d possesses an entangled rubbery plateau for both $T > T_{g,bulk}$ and $T_{g,bulk} > T > T_{g,surf}$, where $T_{g,surf}$ is the glass transition at the free surface; see Fig. S5 in the SI. Consistent with this identification, in bulk the plateau shortens with reducing M_w , disappearing below the M_e of PS, and the plateau height is insensitive to M_w (see Figs. S6 and S7 in the SI). More broadly, the time evolution of d is consistent with entangled polymer dynamics. Pre-plateau, ridge evolution obeys Rouse relaxation, with a $d_t \sim D_t \sim t^{1/2}$ scaling²⁷. The onset of the plateau reflects the Rouse time τ_e of the entanglement strand, after which topological chain entanglements prevent further creep, exhibiting a plateau region with constant height (i.e., $d_{plateau}$; see Inset of Fig. 2a), until the reptation time of the chain τ_{rep} . After this, viscous flow with $d_t \sim t^1$ is recovered via long-time chain escape from their original entanglement networks. The obtained τ_{rep} values at $T > T_{g,bulk}$ share the same temperature dependence with the PS reptation time deduced from the torsional shear experiments³⁵ (Fig. S8). Similar identification is also applicable for the surface creep behaviors at $T < T_{g,bulk}$, as shown in Figs. 2b and S9. Finally, as indicated by the shared Rouse and reptation time temperature dependences (Fig. 2c) and the collapse to a single TTS master curve for data at $T > T_{g,bulk}$ (Fig. 3a), the bulk chain dynamics obey TTS.



In contrast, TTS fails for surface dynamics probed below $T_{\rm g,bulk}$. This is evident in the pronounced decoupling between Rouse and reptation dynamics at the surface shown in Fig. 2c. Unlike bulk dynamics (which are observed to obey a VFT temperature dependence), these surface dynamics can be described by an Arrhenius temperature dependence. The weaker temperature dependence for Rouse than for reptation dynamics ($E_{\rm e,surf} = 134 \, \rm kJ/mol$ for Rouse and $E_{\rm rep,surf} = 269 \, \rm kJ/mol$ for reptation) indicates substantial dynamic decoupling. The consequences of this can be seen in Fig. 3b; the TTS master curve collapse observed in bulk fails near the polymer surface (*i.e.*, surface TTS breakdown). Instead, the plateau breadth grows with cooling. This growth is in contrast to standard entanglement physics, where the plateau breadth is controlled by the ratio of chain to entanglement molecular weights and is thus roughly temperature invariant.

To shed light on the molecular mechanism of this surface TTS breakdown, we performed molecular simulations of dynamics near the free surface of an entangled (192-mer) bead-spring polymer film (see the SI for details). The simplest way of probing dynamics complementary to the experimental results is to compute the segmental mean-square displacement $\langle r^2 \rangle$. Like the creep modulus, $\langle r^2 \rangle$ exhibits distinct scaling regimes corresponding to Rouse, entanglement, and terminal regimes, *via* the relation $\langle r^2 \rangle \sim t^{\lambda}$. Empirically, bulk entangled chains in this molecular weight range exhibit $\lambda \sim 2/5$ in the equivalent of the entanglement plateau regime (see Fig. S10 in the SI), and we employ this as a signature of entanglement-like behavior.

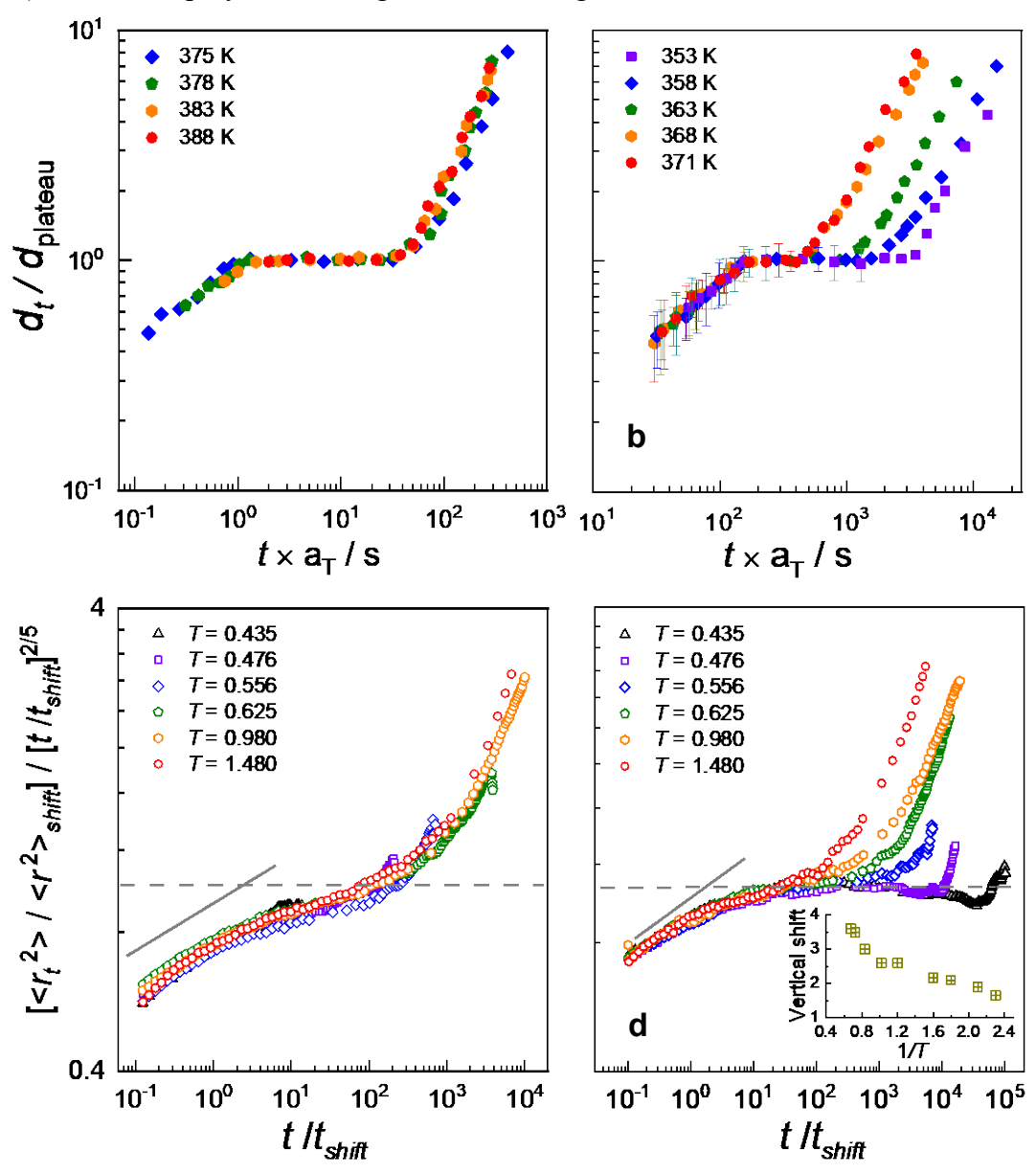


Figure 3

As shown in Fig. 3c, $\langle r^2 \rangle$ in the mid-film obeys TTS as indicated by a collapse of $\langle r^2 \rangle$ data across all temperatures to a master curve (see time-shift factors from simulation in Fig. S11 in the SI) – a result consistent with the bulk experimental data (Fig. 3a). At intermediate times, they exhibit a drop to near (but not quite) a slope of 2/5, reflecting the fact that these chains are lightly entangled. Remarkably, as shown in Fig. 3d, simulations exhibit qualitatively comparable anomalous TTS-breakdown effects at a polymer surface with the experiments: the entanglement regime in $\langle r^2 \rangle$ near the surface exhibits a longer lifetime at lower temperatures than at higher temperature.

In simulation, we can also probe trends in surface stiffness based on the vertical shift factor employed to obtain a collapse shown in Fig. 3d. As shown in Fig. 3d inset, the normalized displacement in the surface layer drops in the entanglement-like regime with decreasing temperature. Because $\langle r^2 \rangle$ is related to stiffness as $G \sim kT/\langle r^2 \rangle$ (G: shear modulus)³⁶, this indicates an enhancement in surface rubbery stiffness on cooling. This contrasts with the usual stiffening of rubbery polymer response on heating.

This suggests that the plateau broadening at the surface in Figs. 2b, 3b and 3d is not a topological entanglement effect, since entanglement densities are generally temperature invariant. Instead, a typical segment near the fast-relaxing surface is part of a chain that extends into the slow-relaxing film interior. Chain segments near the surface relax quickly on a local scale, but then must wait upon relaxation of segments deeper in the film (see Fig. 4a, generated in VMD³⁷). This interfacial transient elastomeric phenomenon is driven by a transient tethering effect emerging from the surface mobility gradient. This explains the surface stiffening on cooling: the effective thickness of the liquid-like mobile region shrinks on cooling^{14,38} as the magnitude of the gradient grows. More importantly, it explains the surface TTS breakdown, as the diffusion lifetime is governed by relaxations deeper in the film that slow on cooling more dramatically than do segmental or Rouse relaxations near the surface.

If this rationale is correct, then surface dynamics for *unentangled* polymers should exhibit a rubbery regime emerging from the transient tethering effect. To enable a quantitative test of this idea, we develop a dynamical mean field theory for motion of an unentangled chain in a dynamical gradient at a film surface (see Methods and SI for theory details). The theory predicts the dynamical consequences of (a) progressive 'tethering' of a near-surface segment to segments deeper in the empirically-observed double-exponential gradient in segmental relaxation times emanating from the free surface and (b) a coexisting harmonic reduction in the length of these tethers with depth in the film — the consequence of a reflecting boundary condition on the first-passage statistics of a random walk³⁹. The theory leads to a set of recursion relations in which the motion of each segment depends on the motion of a tethered segment deeper in the film; it is solved numerically beginning with the most deeply buried segment of a chain contacting the surface.

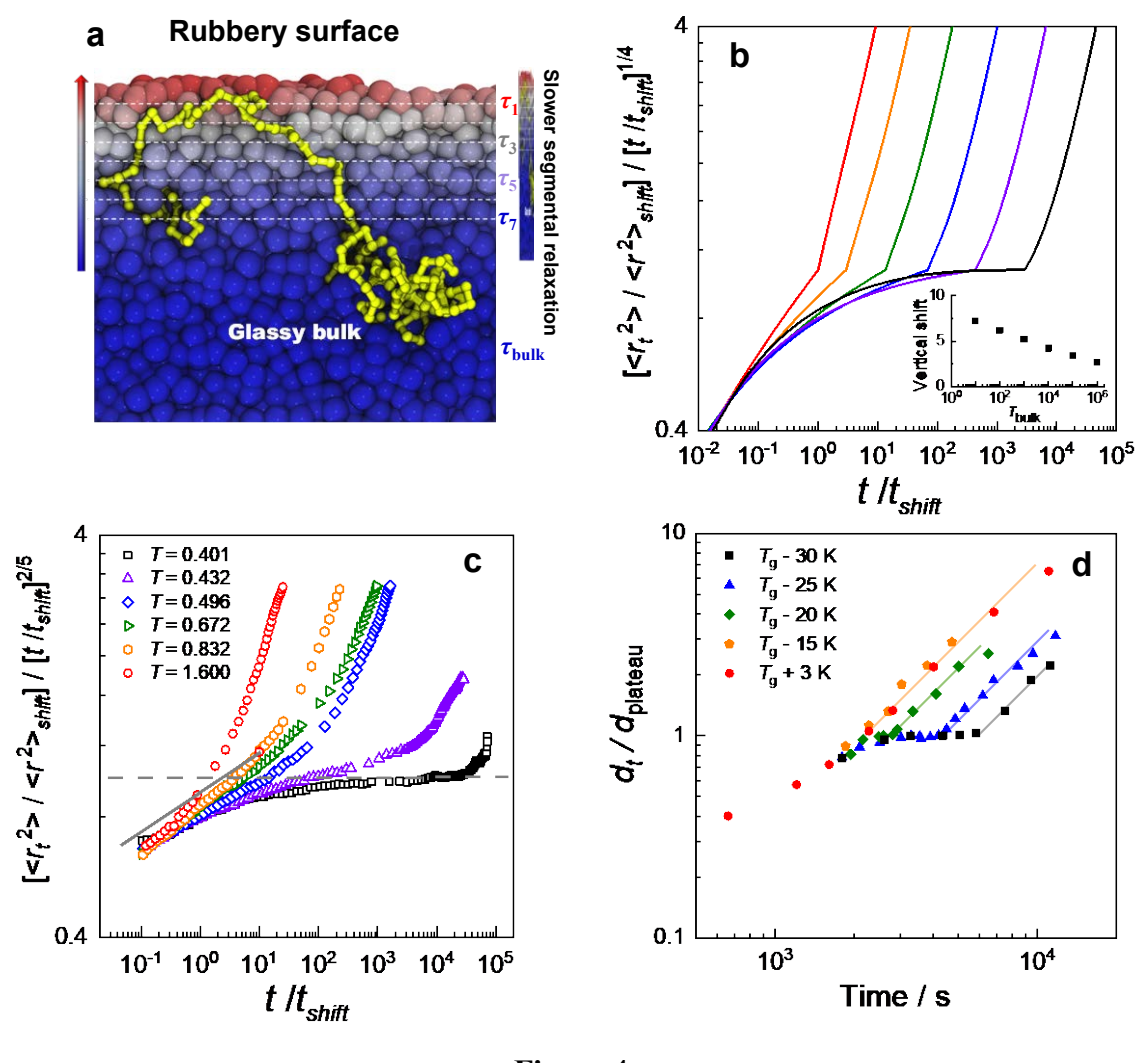


Figure 4

Fig. 4b illustrates key theory predictions for the temperature dependence of surface dynamics in an unentangled, 48-bead chain. No free parameters for chain motion or statistics are invoked; only information on the segmental dynamics gradient is employed from simulation. The theory predicts a progressive emergence of an entanglement-like transient rubbery plateau at the surface upon cooling, consistent with the reasoning above. Within this regime, segmental displacement is predicted to follow an effective t^{1/4} scaling in the bulk relaxation time range relevant to simulation. This scaling exponent is comparable to that for ideal reptation. This difference from the 2/5 exponent reported empirically in simulation (Fig. 3d) is a consequence of the neglect of fluctuations in tether depth. This mirrors a parallel outcome of the mean-field reptation theory for topological entanglement, which incorrectly predicts a scaling exponent of ½ for finite chains due to neglect of chain end fluctuations. Corrections to mean field will be addressed in future work.

5

We test the theory's predictions by performing MD simulations of an unentangled 48-bead polymer film over a comparable temperature range. As shown in Fig. 4c, simulations are in remarkable agreement with theory, with the theory predicting emergence of a surface rubbery regime as bulk relaxation time increases and temperature decreases. The breadth of the plateau at the lowest simulation temperatures is predicted near *quantitatively*. As shown in Fig. 4b inset, the theory also predicts the stiffening, reported in Fig. 3d inset, of the surface rubbery response on cooling, driven by the growing magnitude of the surface dynamical gradient. *As shown in Fig. 4d, remarkably, this predicted that rubbery-like plateau also emerges experimentally at low temperatures at the surface of a subentangled polymer, in qualitative agreement with theory and simulation.*

We emphasize that no *genuine* topological entanglement is implicated in any of these cases: both experiment (Fig. S6) and simulation (Figs. S10 and S12) involve bulk unentangled chains. Analysis of simulations *via* the Z1 algorithm indicates that the effect is *not* associated with a growth of topological entanglements at the surface or on cooling (Figs. S13 and S14); the theory itself does not incorporate *any* genuine entanglement dynamics. Instead, this effect *mimics* that of enhanced entanglement near the surface (*i.e.*, plateau broadening at low *T* and production of surface rubbery state for unentangled polymers). This effect can coexist with previously reported reductions in topological entanglements near interfaces^{40,41}, with an initial reduction in surface rubbery plateau duration at relatively higher temperature (Fig. 2b, c and 3b, d) pointing to a surface reduction in true entanglements that is ultimately more than compensated for by the mobility-gradient induced diffuse tethering effect that leads to the emergence of an interfacial transient elastomeric domain at lower temperature. Results from the Z1 algorithm (Fig. S13) point to consistent findings for simulation.

Evidently, both long and short chain polymers can diffuse at polymer surfaces, but their diffusion is gated by an emergent interfacial 'pseudoentanglement' effect, wherein connectivity to slower relaxing material deeper into the gradient yields transient rubbery-like behavior even in subentangled systems. Therefore, this new mode of slow, transiently rubbery, surface *chain* dynamics emerges precisely because surface *segmental* dynamics are accelerated relative to bulk.

References and Notes:

_

- 1. J. R. Dutcher, M. D. Ediger, Glass surfaces not so glassy. Science 319, 577 (2008).
- 2. R. A. L. Jones, Glasses with liquid-like surfaces. Nat. Mate. 2, 645-646 (2003).
- 3. S. Napolitano, E. Glynos, N. B. Tito, Glass transition of polymers in bulk, confined geometries, and near interfaces. *Rep. Prog. Phys.* **80**, 036602 (2017).
- 4. S. F. Swallen, K. L. Kearns, M. K. Mapes, Y. S. Kim, R. J. McMahon, M. D. Ediger, T. Wu, L. Yu, S. Satija, Organic glasses with exceptional thermodynamic and kinetic stability. *Science* **315**, 353-356 (2007).
- 5. M. D. Ediger, Perspective: highly stable vapor-deposited glasses. *J. Chem. Phys.* **147**, 210901 (2017).
- 6. K. S. Schweizer, D. S. Simmons, Progress towards a phenomenological picture and theoretical understanding of glassy dynamics and vitrification near interfaces and under nanoconfinement. *J. Chem. Phys.* **151**, 240901 (2019).
- 7. C. J. Ellison, J. M. Torkelson, The distribution of glass-transition temperatures in nanoscopically confined glass formers. *Nat. Mater.* **2**, 695-700 (2003).
- 8. R. D. Priestley, C. J. Ellison, L. J. Broadbelt, J. M. Torkelson, Structural relaxation of polymer glasses at surfaces, interfaces, and in between. *Science* **309**, 456-459 (2005).
- 9. J. E. Pye, K. A. Rohald, E. A. Baker, C. B. Roth, Physical aging in ultrathin polystyrene films: evidence of a gradient in dynamics at the free surface and its connection to the glass transition temperature reductions. *Macromolecules* **43**, 8296-8303 (2010).
- 10. L. Yu, Surface mobility of molecular glasses and its importance in physical stability. *Adv. Drug. Deliver Rev.* **100,** 3-9 (2016).
- 11. C. L. Jackson, G. B. McKenna, The glass transition of organic liquids confined to small pores. *J. Non-Crystal. Solids* **131-133**, 221-224 (1991).
- 12. J. L. Keddie, R. A. L. Jones, R. A. Cory, Size-dependent depression of the glass transition temperature in polymer films. *Europhys. Lett.* **27**, 59-64 (1994).
- 13. Z. Fakhraai, J. A. Forrest, Measuring the surface dynamics of glassy polymers. *Science* **319**, 600-604 (2008).
- 14. K. Paeng, S. F. Swallen, M. D. Ediger, Direct measurement of molecular motion in freestanding polystyrene thin films. *J. Am. Chem. Soc.* **133**, 8444-8448 (2011).
- 15. M. D. Ediger, J. A. Forrest, Dynamics near free surfaces and the glass transition in thin polymer films: a view to the future. *Macromolecules* **47**, 471-478 (2014).

- 16. Z. Yang, Y. Fujii, F. K. Lee, C-H, Lam, O. K. C. Tsui, Glass transition dynamics and surface layer mobility in unentangled polystyrene films. *Science* **328**, 1676-1679 (2010).
- 17. Y. Chai, T. Salez, J. D. McGraw, M. Benzaquen, K. Dalnoki-Veress, E. Raphaël, J. A. Forrest, A direct quantitative measure of surface mobility in a glassy polymer. *Science* **343**, 994-999 (2014).
- 18. Y. Li, W. Zhang, C. Bishop, C. Huang, M. D. Ediger, L. Yu, Surface diffusion in glasses of rod-like molecules posaconazole and itraconazole: Effect of interfacial molecular alignment and bulk penetration. *Soft Matter* **16**, 5062-5070 (2020).
- 19. B. M. I. Flier, M. C. Baier, J. Huber, K. Müllen, S. Mecking, A. Zumbusch, D. Wöll, Heterogeneous diffusion in thin polymer films as observed by high-temperature single-molecule fluorescence microscopy. *J. Am. Chem. Soc.* **134**, 480-488 (2012).
- 20. Q. Xu, N. Zhu, H. Fang, X. Wang, R. D. Priestley, B. Zuo, Decoupling role of film thickness and interfacial effect on polymer thin film dynamics. *ACS Macro Letters* **10**, 1-8 (2021).
- 21. M. F. Toney, T. P. Russell, J. A. Logan, H. Kikuchi, J. M. Sands, S. K. Kumar, Near-surface alignment of polymers in rubbed films. *Nature* **374**, 709-711(1995).
- 22. N. Maeda, N. Chen, M. Tirrell, J. N. Israelachvili, Adhesion and friction mechanisms of polymer-on-polymer surfaces. *Science* **297**, 379-382 (2002).
- 23. K. Tanaka, A. Takahara, T. Kajiyama, Rheological analysis of surface relaxation process of monodisperse polystyrene films. *Macromolecules* **33**, 7588-7593 (2000).
- 24. D. Wang, X. Wei, X. Liang, Y. Wu, F. Wang, P. Gong, W. Guan, Y. Wang, Y. Yang, Fast surface dynamics enabled cold joining of metallic glasses. *Sci. Adv.* 5, eaax7256 (2019).
- 25. X. Li, J. Xu, D. Wang, Y. Sha, W. Chen, D. Zhou, X. Wang, Q. Sun, G. Xue, L. Li, Low-temperature processing of polymer nanoparticles for bioactive composites. *J. Polym. Sci. B: Polym. Phys.* **54**, 2514-2520 (2016).
- 26. F. Chen, C-H. Lam, O. K. C. Tsui, The surface mobility of glasses. *Science* **343**, 975-976 (2014).
- 27. M. Rubinstein, R. H. Colby, *Polymer Physics* (Oxford University Press, New York, 2003).
- 28. A. P. Sokolov, K. S. Schweizer, Resolving the mystery of the chain friction mechanism in polymer liquids. *Phys. Rev. Lett.* **102**, 248301 (2009).
- 29. J-H. Hung, J. H. Mangalara, D. S. Simmons, Heterogeneous rouse model predicts polymer chain translational normal mode decoupling. *Macromolecules* **51**, 2887-2898 (2018).

- 30. A. Carré, J.-C. Gastel, M. E. R. Shanahan, Viscoelastic effects in the spreading of liquids. *Nature* **379**, 432-434 (1996).
- 31. M. E. R. Shanahan, A. Carré, Spreading and dynamics of liquid drops involving nanometric deformations on soft substrates. *Colloids Surf. A* **206**, 115-123 (2002).
- 32. E. R. Jerison, Y. Xu, L. A. Wilen, E. R. Dufresne, Deformation of an Elastic Substrate by a Three-Phase Contact Line. *Phys. Rev. Lett.* **106**, 186103 (2011).
- 33. H. Lu, W. Chen, T. P. Russell, Relaxation of thin films of polystyrene floating on ionic liquid surface. *Macromolecules* **42**, 9111-9117 (2009).
- 34. L. J. Fetters, D. J. Lohse, D. Richter, T. A. Witten, A. Zirkel, Connection between polymer molecular weight, density, chain dimensions, and melt viscoelastic properties. *Macromolecules* **27**, 4639-4647 (1994).
- 35. D. J. Plazek, V. M. O'Rourke, Viscoelastic behavior of low molecular weight polystyrene. *J. Polym. Sci: A-2. Polym. Phys.* **9,** 209-243 (1971).
- 36. J. Yang, K. S. Schweizer, Glassy dynamics and mechanical response in dense fluids of soft repulsive spheres. II. Shear modulus, relaxation-elasticity connections, and rheology. *J. Chem. Phys.* **134**, 204909 (2011).
- 37. W. Humprey, A. Dalke, K. Schulten, VMD Visual Molecular Dynamics. *J. Mol. Graph.* **14,** 33-38 (1996).
- 38. R. J. Lang, D. S. Simmons, Interfacial dynamic length scales in the glass transition of a model freestanding polymer film and their connection to cooperative motion. *Macromolecules* **46**, 9818-9825 (2013).
- 39. M. Khantha, V. Balakrishnan, First passage time distributions for finite one-dimensional random walks. *Pramana* **21,** 111-122 (1983).
- 40. L. Si, M. V. Massa, K. Dalnoki-Veress, H. R. Brown, R. A. L. Jones, Chain entanglement in thin freestanding polymer films. *Phys. Rev. Lett.* **94,** 127801 (2005).
- 41. H. R. Brown, T. P. Russell, Entanglements at polymer surfaces and interfaces. *Macromolecules* **29**, 798-800 (1996).

Figure Legends:

- Fig. 1. Formation of wetting ridge and its topological profile. (a) Diagrams showing the formation of a wetting ridge by an ionic liquid droplet on a PS surface at different temperature ranges and the corresponding mobile regions; (b), (c) AFM topological images showing the profile of the wetting ridge on a PS surface formed at 380 $(T_{g,bulk} + 6 \text{ K})$ and 368 K $(T_{g,bulk} 6 \text{ K})$ (t = 2230 s). (d) and (e) Representative cross-sectional AFM images showing changes of the wetting ridge profile with t at 383 $(T > T_{g,bulk})$ and 363 K $(T_{g,surf} < T < T_{g,bulk})$, respectively. (γ_l is surface tension of liquid; θ is apparent contact angle).
- Fig. 2. Polymer nano-rheology and surface chains dynamics. (a), (b) Time evolution of the $d_t/d_{plateau}$ at $T > T_{g,bulk}$, reflecting bulk dynamics, and $T_{g,bulk} > T > T_{g,surf}$ (surface dynamics). $d_{plateau}$ is the d values at the plateau region and $d_t/d_{plateau} \sim D_t/D_R$ (D_R : rubbery compliance). (c) Dependence of the bulk ($\tau_{e,bulk}$ and $\tau_{rep,bulk}$) and surface ($\tau_{e,surf}$ and $\tau_{rep,surf}$) relaxation time on temperature. Curves at $T > T_{g,bulk}$ represent the fitting results of bulk dynamics by Vogel-Fulcher-Tamann (VFT) law: $ln\tau = ln\tau_0 + B/(T T_k)$, with $\tau_{e,bulk}$: $T_k = 323$ K, $B_e = 1303$; $\tau_{rep,bulk}$: $T_k = 322$ K, $T_{rep,bulk}$: $T_k = 322$ K, $T_k = 322$
- Fig. 3. Failure in time-temperature superposition (TTS) law at glassy polymer surface. (a) Master curve of $d_t/d_{plateau}$ vs t relationships showing the successful TTS for bulk dynamics ($T_r = 388$ K); (b) an inadequate superposition of the curves indicating TTS-breakdown in polymer surface dynamics ($T_r = 371$ K). T_r is the reference temperature. The error bars represent 1s.d. (c) Master curve collapse of simulated $< r^2 > /t^{2/5}$ data vs time for chain segments in the bulk-like mid-film. (d) Breakdown of master curve collapse for the same quantities in a 1-segment-thick layer at the surface of the film. Gray solid lines in (c) and (d) show the expected scaling in the Rouse regime; dashed curves denote a value of 1. Here vertical shifts collapse the plateau and horizontal shifts collapse the Rouse time. Inset of panel d displays the trend of decreasing vertical shift factor (stiffening) with cooling.
- Fig. 4. Emergence of rubbery state at the surface of unentangled polymer. (a) Illustration of the creation of interfacial transient elastomer domain at the surface via the segmental dynamic gradient, employing representative simulation snapshot (rendered in VMD³⁷). The exponential gradient in activation barriers to relaxation is illustrated by the color gradient of background beads; a representative chain spanning from the surface to the mid-film is highlighted in yellow. This gradient-spanning strand produces the transient surface rubbery behavior. (b) Master curve collapse of predictions of normalized mean-square-displacement vs normalized time from the Mean-Field Surface "Pseudoentanglement" Theory (see the SI for details). From left to right, curves correspond to bulk relaxation times of 10^0 , 10^1 , 10^2 , 10^3 , 10^4 , and 10^5 Lennard Jones timesteps. Inset shows the vertical shift factor producing this collapse, indicating a prediction of stiffening on cooling. (c) Breakdown of TTS master curve collapse, as in Fig. 3d, of simulated $< r^2 > /t^{2/5}$ data vs time for chain segments in a 1-segment-thick layer at the surface of the film (48-mer chain). Gray solid lines show the expected scaling in the Rouse regime; dashed curves denote a value of 1. (d) Master curves of $d/d_{plateau} vs$ t relationships for an unentangled PS ($M_w = 11 \text{ kg/mol}$) ($T_r = T_g + 3 \text{ K}$).

Methods

Experiment: The sample information and physical characteristics of the PS and [EIm]BF₄ ionic liquid can be found in the SI. The surface nano-creep experiments utilized the surface tension of [EIm]BF₄ droplets atop PS surface to draw the surface up, forming a well-defined ridge-like deformation (*i.e.*, wetting ridge). The time-dependence of the height of wetting ridge at $T > T_g^{\text{bulk}}$ reflects polymer bulk mechanics, while that at $T < T_g^{\text{bulk}}$ reveals the surface viscoelasticity. In a representative experimental procedure, a PS film of 600 nm thickness was prepared by spin-coating onto a silicon wafer surface, annealed at 414 K for 24 h to remove residual solvents, and mounted onto a hot stage set to a specific temperature. Subsequently, a 3 μ L volume of ionic liquid was deposited onto the film surface to form a microdroplet with a contact angle about $72 \pm 3^{\circ}$ and left to set for a desired time t, during which the wetting ridge was allowed to grow. At the end of time t, the PS film was quenched to freeze in its morphology. Then the film was warmed slowly to room temperature so that the droplet could be removed, and then subjected to an atomic force microscopy (AFM; Bruker Multimode-8 mode) measurement to assess the topological profile of the wetting ridge.

Simulation methods and full theoretical development can be found in the supplementary material.

Theory: In summary, the theory considers the motion of a subentangled chain placed in a gradient of segmental relaxation times at the surface of a film. In the bulk, the chain would obey Rouse motion. However, at the surface, the displacement of a segment at a position z_i is constrained by a covalent tether to a segment at a deeper position z_i . Employing an assumption of Gaussian chain statistics together with a first passage analysis yields a tether length of $R_{\parallel}^{2}(z_{i},z_{j}) = 2(z_{j}^{2}-z_{i}^{2})$. The tagged segment at z_i then obeys Rouse motion at a rate determined by its local segmental friction coefficient, until it feels the constraint of its tether, which occurs at a time $t^*(z_i,z_i)$ when it traveled the root mean square in-plane end-to-end distance: $\left\langle r^{2}\left(z_{i}, t^{*}\left(z_{i}, z_{j}\right)\right)\right\rangle = R_{\parallel}^{2}\left(z_{i}, z_{j}\right) + \left\langle r^{2}\left(z_{j}, t^{*}\left(z_{i}, z_{j}\right)\right)\right\rangle$. At longer times $t > t^{*}$ further dispacement occurs at the rate of the tether point at z_j ; i.e. $\langle r^2(z_i,t)\rangle = \langle r^2(z_j,t)\rangle + R_{\parallel}^2(z_i,z_j)$ for $t > t^*(z_i,z_j)$. The theory is solved numerically in a recursive manner beginning at the most deeply embedded segment (which obeys Rouse motion at a rate determine by its local segmental friction coefficient) and working recursively towards the surface. Further details of the theoretical development can be found in the Supplementary Theoretical Development section of the Supplementary Information.

<u>Simulation details:</u> Methodological details of the simulations can be found in the Supplementary Simulation Methods section of the SI.

Data availability: The data that support the findings of this study are available within the article and its Supplementary Information. Raw simulation trajectories are available upon request from D.S.S.

Code availability: Simulations employ standard codes (LAMMPS) and methods that are freely available or documented in the literature.

Acknowledgments: B.Z. acknowledge financial support from Natural Science Foundation of China (Grant nos. 21973083 and 21504081), and R.D.P and K.R. acknowledge support from National Science Foundation (NSF) Materials Research Science and Engineering Center Program through the Princeton Center for Complex Materials (DMR-1420541 and DMR-2011750) and the NSF through CBET-1706012. D.S.S. and A.G. acknowledge support from the National Science Foundation through grant number CBET-1854308. X.W. thanks the Natural Science Foundation of China (Grant nos. 21674100 and 21873085), and K.T. acknowledges the JST-Mirai Program (JPMJMI18A2). The authors thank Dr. Norifumi L. Yamada for assisting the neutron reflectivity measurements and Prof. O. K. C. Tsui and J. J. Zhou for fruitful discussion.

Author contributions: B.Z. and R.D.P. conceived and supervised the experiments. Z.H., N.Z., and K.R. performed experiments. D.S.S. and A.G. conceived and analyzed all simulations and theories; A.G. performed all simulations under D.S.S. supervision. D.K and K.T. provided data from neutron reflectivity. All authors discussed results and wrote the manuscript.

Competing interests: The authors declare no competing financial interests.

Additional Information: Supplementary Information is available for this paper; Correspondence and requests for materials should be addressed to B.Z., D.S.S and R.D.P.

Reprints and permissions information is available at www.nature.com/reprints.

Supplementary information for

Mobility Gradients Yield Rubbery Surfaces atop Polymer Glasses

Zhiwei Hao^{1,†}, Asieh Ghanekarade^{2,†}, Ningtao Zhu¹, Katelyn Randazzo³, Daisuke Kawaguchi⁵, Keiji Tanaka^{5,6}, Xinping Wang¹, David S. Simmons^{2,*}, Rodney D. Priestley^{3,4,*}, and Biao Zuo^{1,*}

Affiliations:

- ¹ Department of Chemistry, Key Laboratory of Surface & Interface Science of Polymer Materials of Zhejiang Province, National Engineering Lab for Textile Fiber Materials and Processing Technology (Zhejiang), Zhejiang Sci-Tech University, Hangzhou, China.
- ² Department of Chemical and Biomedical Engineering, University of South Florida, Tampa, Florida, United States.
- ³ Department of Chemical and Biological Engineering, Princeton University, Princeton, New Jersey, United States.
- ⁴ Princeton Institute for the Science and Technology of Materials, Princeton University, Princeton, New Jersey, United States.
- ⁵ Department of Applied Chemistry, Center for Polymer Interface and Molecular Adhesion Science, Kyushu University, Fukuoka, Japan.
- ⁶ International Institute for Carbon-Neutral Energy Research (WPI-I2CNER), Kyushu University, Fukuoka, Japan.

*Correspondence to: <u>dssimmons@usf.edu</u> (for DSS); <u>rpriestl@princeton.edu</u> (for RDP) <u>chemizuo@zstu.edu.cn</u> (for BZ)

This PDF file includes:

Supplementary Theoretical Development Supplementary Simulation Methods Supplementary Data Tab. S1 Figs. S1 to S16 Supplementary References

[†]These authors contributed equally to this work.

Supplementary Theoretical Development

In order to obtain a leading-order mean field theory of of the emergence of an interfacial transient elastomeric domain, we employ a minimal dynamical model of a polymer chain: in the bulk, the chain obeys sub-diffusive Rouse dynamics at all times less than the Rouse time of the whole chain and exhibits a restoration of diffusive dynamics at longer times. We do not explicitly model the segmental relaxation process itself, although we treat the segmental alpha relaxation time τ as setting the rate of Rouse subdiffusion:

$$\langle r^2(t) \rangle = \left(\frac{t}{\tau}\right)^{1/2} \quad t < \tau_{\text{Rouse}}$$
 (1)

We consider the motion of such a chain, of length n, placed near the surface of a film within the surface gradient in segmental relaxation time, $\tau(z,T)$. Prior work has shown this gradient to be of a double exponential form¹⁻⁹:

$$\tau(z,T) = \tau_{bulk}(T) \exp\left[-A(T) \exp\left(-\frac{z}{\xi}\right)\right]$$
 (2)

where $\tau_{bulk}(T)$ is the bulk segmental relaxation time at a temperature T, A(T) is a temperature-dependent parameter that sets the magnitude of the gradient at temperature T, and ξ is a range parameter that is at most weakly temperature-dependent. Prior work has established the temperature variation of $A(T)^{1,10,11}$:

$$A(T) = \varepsilon_0 \ln \frac{\tau_{bulk}(T)}{\tau^*}$$
 (3)

Here ε_0 is a constant reflecting the fractional reduction in the activation barrier for segmental relaxation at the surface relative to bulk, and τ^* is an onset timescale for the segmental relaxation time gradient. In practice τ^* has a weak z-dependence that is relevant to quantitative prediction⁹, but here we treat this quantity as constant for the purposes of a leading-order treatment. Prior simulation results in this model suggest $\varepsilon \cong 0.8$, $\xi \cong 4$, and $\tau^* \cong 1$ $\tau_{\rm LJ}$. We employ these values below in making quantitative theory predictions^{10,11}.

We now consider the mean square displacement of a segment at a distance z_1 from the surface. At short times, this segment obeys Rouse subdiffusion as in the bulk, albeit at a rate determined by the local relaxation time:

$$\left\langle r^{2}\left(z_{1},t\right)\right\rangle =\left(\frac{t}{\tau\left(z_{1}\right)}\right)^{1/2}$$
 (4)

However, at long times this segment's motion is constrained by a tether to a segment deeper in the film at position $z_2 > z_1$. We compute the number of segments in this tether by modeling it as a one-dimensional random walk from z_1 to z_2 , with a reflecting boundary condition at z = 0. The expectation value $E[n(z_1 \rightarrow z_2)]$ for this number of steps is given via a first-passage analysis by the equation 12

$$E[n(z_1 \to z_2)] = \frac{z_2^2 - z_1^2}{a_2^2} = \frac{z_2^2 - z_1^2}{a^2/3}$$
 (5)

where a_z is the average step size in the z direction and a is the bond length. In the in-plane direction, this tether is a random walk obeying Gaussian chain statistics, and it thus has mean in-plane end-to-end length of

$$R_{\parallel}^{2} = a_{\parallel}^{2} n = \frac{2}{3} a^{2} n \tag{6}$$

If we treat this mean end-to-end length as the in-plane length of the tether, we thus expect the mean square in-plane tether length to be equal to

$$R_{\parallel}^{2}(z_{1}, z_{2}) = 2(z_{2}^{2} - z_{1}^{2}) \tag{7}$$

Because Rouse subdiffusion of the segment at z_1 is innately faster than that at z_2 (because of the dynamical gradient in segmental relaxation times), beyond some time $t^*(z_1, z_2)$ the motion of the segment at z_1 will be restricted by this tether. This occurs approximately at the time t^* at which

$$\langle r^2(z_1, t^*(z_1, z_2)) \rangle = R_{\parallel}^2(z_1, z_2) + \langle r^2(z_2, t^*(z_1, z_2)) \rangle$$
 (8)

At longer times, the segment at z_1 displaces at the same rate as the segment at z_2 , since further motion of the segment at z_2 is now the rate limiting step for the segment at z_1 .

$$\left\langle r^{2}\left(z_{1},t\right)\right\rangle =\begin{cases} \left(\frac{t}{\tau\left(z_{1}\right)}\right)^{1/2} & t < t^{*}\left(z_{1},z_{2}\right)\\ \left\langle r^{2}\left(z_{2},t\right)\right\rangle + R_{\parallel}^{2}\left(z_{1},z_{2}\right) & t \geq t^{*}\left(z_{1},z_{2}\right) \end{cases}$$
(9)

The motion of the segment at z_2 is then further constrained by a yet deeper segment at z_3 , such that at times longer than $t^*(z_2, z_3)$ its motion is likewise restricted. Similarly, that segment is restricted by a yet deeper segment, and so on. We thus have in general a recursive equation relating layers nearest the interface to layers deeper in the film:

$$\left\langle r^{2}\left(z_{i},t\right)\right\rangle =\begin{cases} \left(\frac{t}{\tau\left(z_{i}\right)}\right)^{1/2} & t < t^{*}\left(z_{i},z_{j}\right) \\ \left\langle r^{2}\left(z_{j},t\right)\right\rangle + R_{\parallel}^{2}\left(z_{i},z_{j}\right) & t \geq t^{*}\left(z_{i},z_{j}\right) \end{cases}$$
(10)

with $t^*(z_i,z_i)$ defined as

$$\left\langle r^{2}\left(z_{i}, t^{*}\left(z_{i}, z_{j}\right)\right)\right\rangle = R_{\parallel}^{2}\left(z_{i}, z_{j}\right) + \left\langle r^{2}\left(z_{j}, t^{*}\left(z_{i}, z_{j}\right)\right)\right\rangle, \tag{11}$$

with

$$R_{\parallel}^{2}\left(z_{i}, z_{j}\right) = 2\left(z_{j}^{2} - z_{i}^{2}\right) \tag{12}$$

and where this relation must be satisfied for all $z_i > z_i$.

For a chain of finite length, this recursive relation can be solved by beginning at the position Z of the segment furthest from the interface and considering small sequential steps of size Δz nearer to the surface. The segment at Z displaces at all times less than the relaxation time of the full chain via the Rouse scaling, because it is not tethered to anything deeper in thin film:

$$\langle r^2(t,Z)\rangle = \left(\frac{t}{\tau(z=Z)}\right)^{1/2}$$
 for all $t < \tau_{Rouse}$. (13)

Each layer k closer to the surface then displaces according to equation (10), with $z_i = Z - k\Delta z$ and $z_j = Z - (k-1)\Delta z$. Since the fluid is not genuinely comprised of discrete layers, Δz can be made arbitrarily small to converge to the continuous limit. We determine Z for a chain of length n by employing equation (5) and determining the largest value z = Z to which the mean first-passage number of steps from the surface (z = 0) is less than or equal to n:

$$Z = a\sqrt{\frac{n}{3}} \tag{14}$$

The final consideration needed is the question of the effective Rouse time of the entire chain – the time of escape to fully diffusive dynamics. We approximate the chain Rouse time as the time at which the mean square displacement, average over all layers involved in the recursion relation above, is equal to the square gyration radius of the chain in the bulk ideal state, $a^2n/6$, where a is the bond length. We solve the system of recursive equations (10) numerically, identifying the crossover to Rouse dynamics via the above criterion numerically. We choose a small value of Δz and confirm that results are not sensitive to this choice in this low- Δz range.

Supplementary Simulation Methods

Simulations employ an attractive bead-spring model extended from the work of Kremer and Grest¹³. Within this model, non-bonded beads interact via the 12-6 Lennard-Jones (LJ) potential, with energy parameter $\varepsilon=1.0$ and range parameter $\sigma=1.0$, with interactions cut off at a distance of 2.5. Bonds are represented via the Finitely Extensible Nonlinear Elastic (FENE) potential, with K=30, $R_0=1.3$, $\varepsilon_{\rm bond}=0.8$, and $\sigma_{\rm bond}=1.0$. This specific forcefield has been used to study dynamics in confined polymers in prior work ^{14,15}, with similar potentials employed in a large body of simulation work probing glass formation in polymers ^{16,17,18}. Simulations are performed in LAMMPS¹⁹.

Data in the main text reflects simulations of chains of length 48 and 192 repeat units. These chains correspond to 0.6 and 2.3 times the entanglement length for this chain, which is reported to be 84 repeat units²⁰. In each case, we simulate films of thickness approximately 26 σ , with lateral dimensions of $26\sigma_{LJ} \times 26\sigma_{LJ}$ to prevent any potential lateral confinement effects.

Simulations of the film comprised of 192-bead chain were performed as follows. Configurations were initiated by placing each chain on a lattice and then inserting chains randomly into the box. These configurations were then annealed isothermally at a reduced LJ temperature of 1.6 for 5 \times 10⁵ $\tau_{\rm LJ}$, where $\tau_{\rm LJ}$ is the LJ unit of time. Because the box size during this step is held constant and is considerably larger than

required by the equilibrium density of the polymer, the polymer rapidly collapses into a film and then thermally anneals.

From here, we employed a recently published iterative quench protocol. Specifically, we performed an isobaric temperature quench of the system described above to a temperature of 1.0, saving several temperatures along the way. We then isothermally equilibrated the configuration at each of these temperatures for 10^6 $\tau_{\rm LJ}$. We then perform a further quench from the annealed T=1.0 sample, targeting a range over temperature over which the relaxation time is expected to increase by an order of magnitude. These temperatures were also annealed for 10^6 $\tau_{\rm LJ}$. This process is then iterated down to the lowest temperatures probed in the study.

The mean end-to-end reorientational relaxation time $<\tau_{\rm ee}>$ of the polymer in the film at the initial temperature of T = 1.6 is $10^{3.8} \tau_{LJ}$ and is $10^{3.9} \tau_{LJ}$ in an equivalent bulk simulation; the chain's end to end vector thus has sufficient time to relax over 60 times and for the chain reach conformational equilibrium in the initial high-temperature equilibration. With the protocol described above, the isothermal annealing period is at least 10 times $\langle \tau_{ee} \rangle$ down to a temperature of 0.714, and at least equal to $\langle \tau_{ee} \rangle$ down to a temperature of approximately 0.59. At lower temperatures reported, the annealing period is at least 10 times the segmental relaxation time, which recent work has demonstrated is more than sufficient to yield equilibrium glassy dynamics in this model¹⁸. Moreover, chain conformational statistics of the freely-jointed bead-spring polymer are approximately temperature invariant 21 , 22 (similarly to experimental polymers), such that chain conformations are expected to reflect equilibrium behavior even at these lower temperatures. This approach is an extension of the recently developed Predictive Stepwise Quench (PreSQ) protocol²¹.

In simulations of the subentangled 48-bead chain, this procedure is slightly modified. Instead of employing a fixed isothermal annealing period of $10^6 \tau_{LJ}$ at each temperature, we anneal for a period of approximately $10 < \tau_{ee} >$ down to the lowest temperature at which this remains possible within a maximum annealing period of $10^6 \tau_{LJ}$ (a temperature of 0.465). At lower temperatures we again employ a fixed annealing period of $10^6 \tau_{LJ}$ and again ensure that equilibration times are at least 10 times the segmental relaxation time. The lowest temperature simulation performed through these simulations each required approximately 20 days of continuous simulation on a compute unit comprised of 8 3.0 GHz cores and a single GTX 1080 Ti GPU.

We analyze dynamics based on the mean square displacement $\langle r^2 \rangle$, computed as

$$\langle r^2(t)\rangle = \frac{1}{S} \sum_{i=1}^{S} \frac{1}{N} \sum_{i=1}^{N} \left[r_i(s_j + t) - r_i(s_j) \right]^2$$

where s_j is the start time of observation, t is the time of displacement, N is the number of particles, and S is the number of start times over which $\langle r^2(t) \rangle$ is averaged. In order to analyze dynamics locally within the film, rather than averaging over all particles in the film, we average over subsets of segments selected based on their distance from the surface at time s. When reporting surface dynamics, we average only over segments that at time s are within a distance of 1 σ_{LJ} of the surface. When reporting mid-film dynamics, we average only over segments that at time s are in the central 1 σ_{LJ} of the film.

As described in the main text, in analyzing the data we consider the time dependent value of the scaling exponent λ in the relation $\langle r^2(t) \rangle \sim t^{\lambda}$. In the simulations Rouse and terminal regimes correspond to $\lambda \cong \frac{1}{2}$ and 1, respectively²³. Unlike in creep, in $\langle r^2 \rangle$ the entanglement regime does not correspond to a flat plateau, but rather to $\lambda \cong \frac{1}{4}$ in the idealized infinite molecular weight limit. Here, however, we simulate finite chains comprised of 192 beads, which as noted above is only 2.3 times the reported entanglement molecular weight for this model. For finite molecular weight chains in simulation, observed whole chain values of γ computed in the entanglement regime are empirically slightly larger due to chain-end effects; the idealized value of $\frac{1}{4}$ is generally only observed in simulation if $\langle r^2(t) \rangle$ calculations are limited to

only a few central beads (for example, 5 central beads) within the chain²³.

Because here we seek to quantify local dynamics within a narrow spatial region near or far from the surface of the film, an additional restriction to a small number of central repeat units would not yield sufficient statistical power. We thus analyze all beads and employ an empirical value of λ based on a calculation for the whole chain. To determine an appropriate whole-chain value of λ in this molecular weight range, we performed supplementary simulations of bulks samples comprised of 48-bead, 192-bead and 288-bead chains. As shown in Fig. S10., we find $\lambda \cong 2/5$ for dynamics in this crossover molecular weight range of light entanglement and we thus use this scaling as an empirical signature of entangled dynamics in these simulations. To better compare the results of this approach to experiment, we rescale $\langle r^2 \rangle$ by this $t^{2/5}$ factor in the main text, as this normalized mean-squaredisplacement is expected to exhibit a plateau in the entanglement regime.

We additionally simulate and analyze dynamics for a subentangled 48-bead chain. Surface dynamics for this system are shown in the main text. Successful collapse of mid-film (bulk-like) data to a single time-temperature superposition (TTS) master curve is shown in Fig. S12.

Supplementary Data

Materials: Mono-dispersed PS was purchased from Polymer Source Co. ltd. (Canada), and the [EIm]BF₄ ionic liquid was supplied by Lanzhou Institute of Physical Chemistry, Chinese Academy of Sciences. The physical parameters of [EIm]BF₄ are listed in Tab. S1. The [EIm]BF₄ is extremely stable at temperatures below 686 K. The zero saturated vapor pressure ensures the invariance of droplet volume and profile during the long-time experiments (also see evidences in Fig. S1). The high surface tension (γ_l) guarantees the formation of a hemisphere droplet (i.e., non-wetting state) atop the PS surface with a contact angle (θ) of 72 ° (see Fig. S1), which creates considerable upward pulling force ($\gamma_l \sin \theta$) at the three-phase line to deform the surface (see Fig. 1 in the main text). As well, since the [EIm]BF₄ is water-soluble, it is immiscible with PS, a hydrophobic polymer. No interfacial swelling or plasticization effects were observed with PS (Figs. S2-S4). These characteristics render [EIm]BF₄ a good testing liquid for our creep experiments at the PS surface at a temperature ranging from 320 to 390 K.

Tab. S1. Physical parameters of [EIm]BF4

Sample	Water Solubility	Surface tension (298 K)	Saturated vapor pressure	Decomposition temperature
1-ethyl-3-methylimidazolium tetrafluoroborate ([EIm]BF 4)	Good	49 mN/m	~ 0	686 K

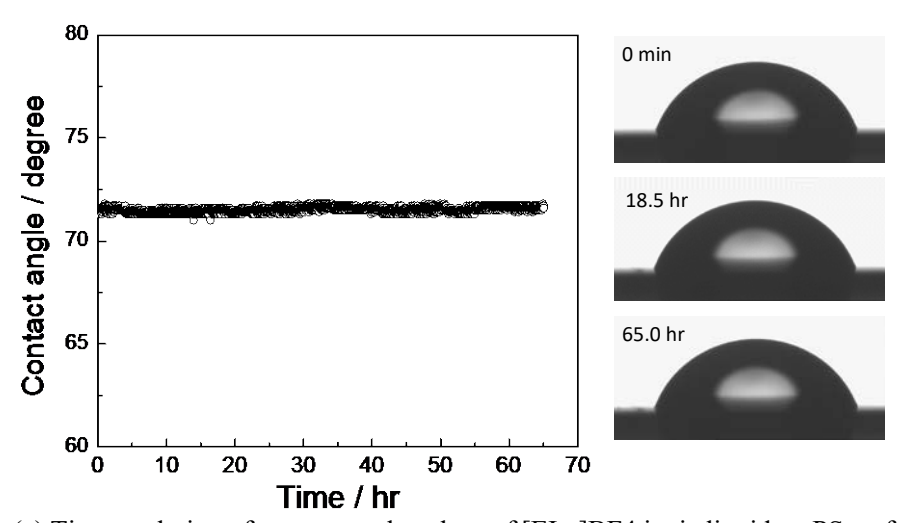


Fig. S1. (a) Time evolution of contact angle values of [EIm]BF4 ionic liquid on PS surface; (b) images showing the unaltered droplet profiles with time (T = 385 K). It is clear that the contact angle values and profile of the liquid droplet did not vary with time, ensuring a long-time creep experiment on polymer surface.

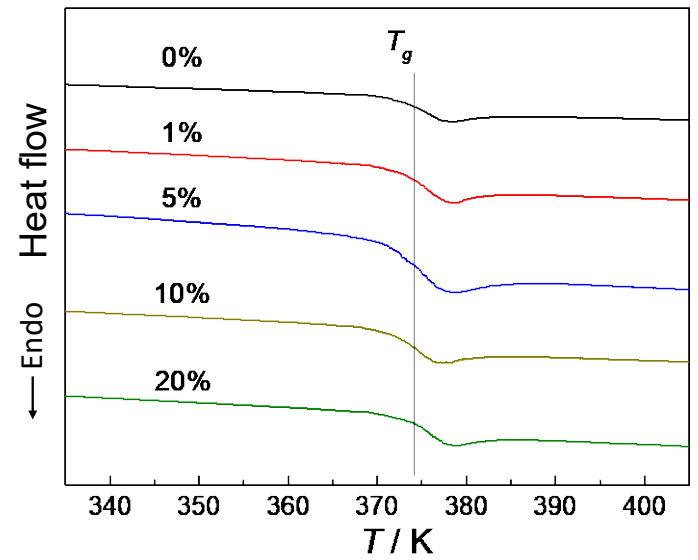


Fig. S2. (a) Differential scanning calorimetry (DSC) curves showing the unchanged $T_{\rm g}$ of the PS blended with [EIm]BF4. This means that the [EIm]BF4 does not plasticize PS.

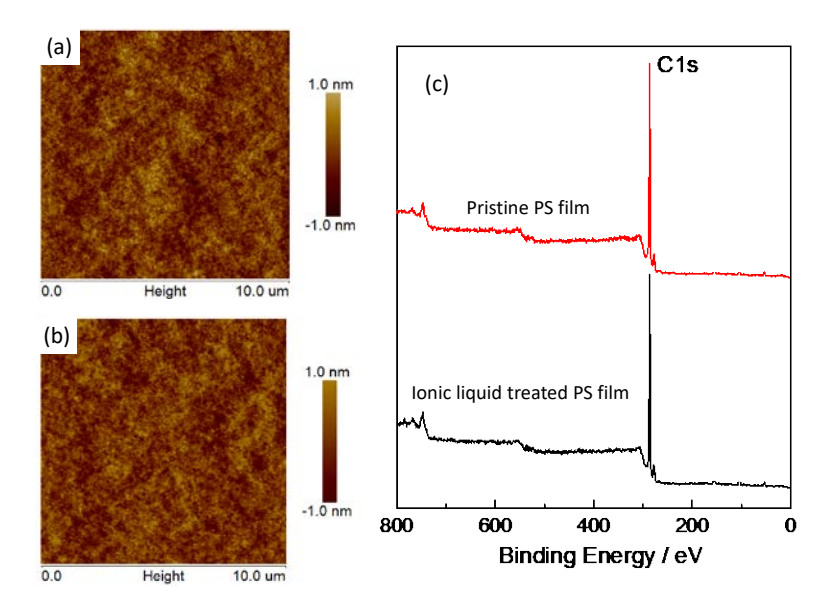


Fig. S3. (a, b) AFM topological images and (c) X-ray photoelectron spectroscopy (XPS) spectra for PS films before and after soaking in ionic liquid for 30 min at 385 K. The results showed that the polymer surface remains smooth and intact (panel a, b), and ionic liquid diffusions are not evident (panel c) after the films were contacted with ionic liquid.

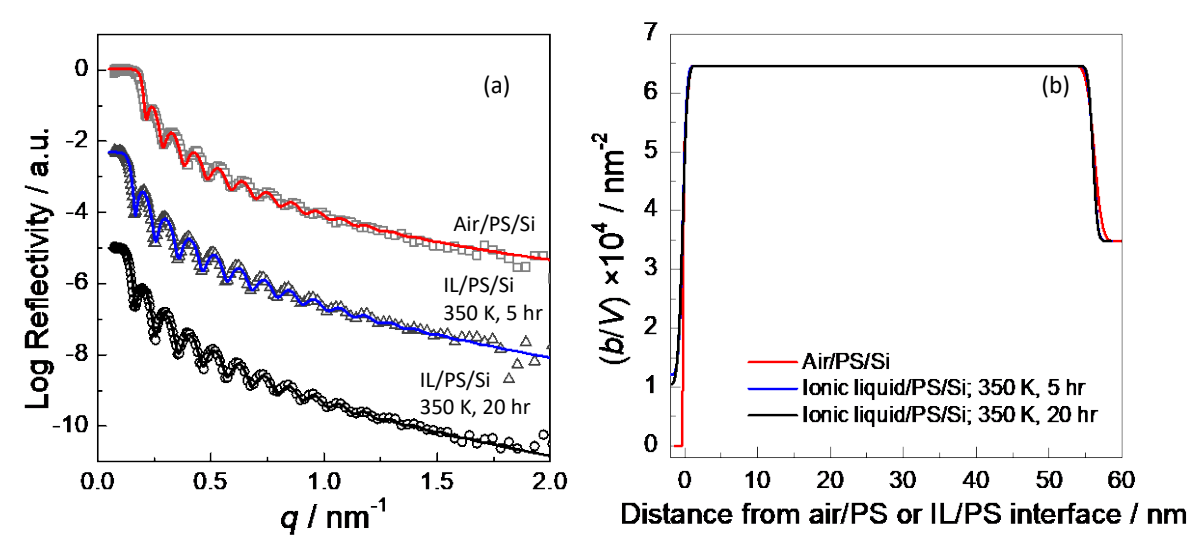


Fig. S4. (a) Neutron reflectivity for a deuterated PS film collected in air at room temperature and in a direct contact with the ionic liquid (IL) at 350 K after equilibrating for 5 and 20 hr. The solid curves represent the reflectivity calculated on the basis of the scattering length density (b/V) profiles shown in (b). For clarity, the curves in panel (a) are offset from one another on the y axis. Notably, except for slight differences in the top surface region due to the different b/V values for air and IL, the b/V profiles of PS films in air and in ionic liquid remain almost the same, and not any interfacial broadening between IL and PS was detected, as shown in panel (b). This means that IL molecules did not diffused into the surface region of PS within our experiment time and temperature ranges.

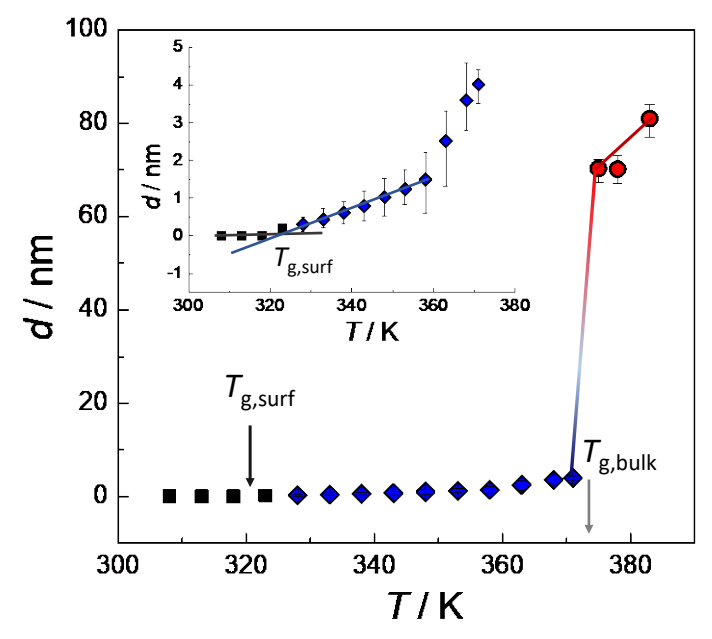


Fig. S5. Variations of the height of wetting ridge (d) with temperature, showing the start of wetting ridge formation at $T_{\rm g,surf}$ (about 320 K) and sharp increase in d near $T_{\rm g,bulk}$. The inset is the enlarged image showing the definition of $T_{\rm g,surf}$. Below ca. 320 K, all deformation ceases, pointing to the vitrification of the surface layer below a surface $T_{\rm g}$ (i.e., $T_{\rm g,surf.} \sim 320$ K). The d values in this figure were acquired after exposing the PS film surface to the ionic liquid for 200 s at various temperatures. Each data point represents averaged results from several measurements at a specific temperature.

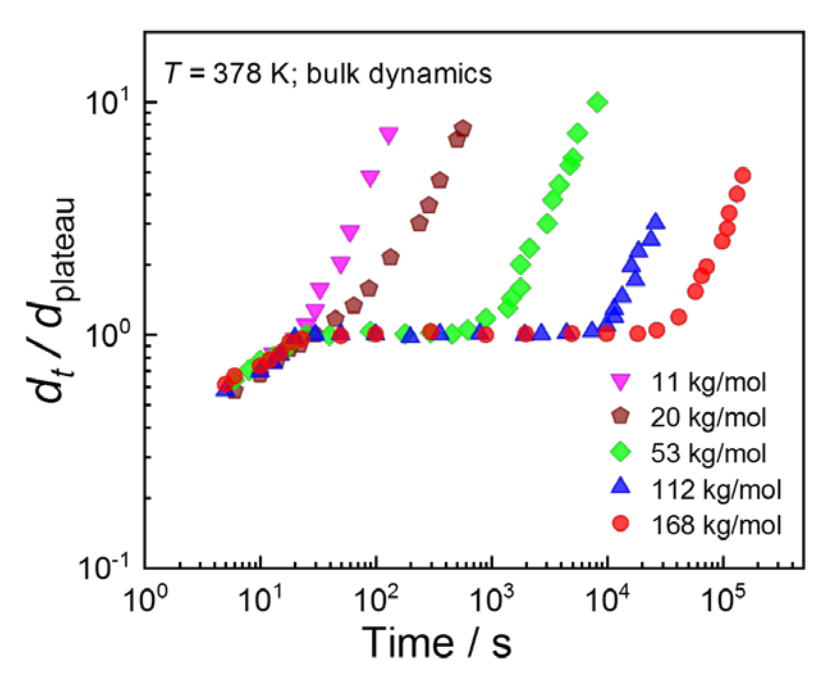


Fig. S6. Height of wetting ridge (d) as functions of creep time for PS film with various molecular weights (T = 378 K). The plateau disappears upon reducing the PS molecular weight to below 20 kg/mol, which is close to the entanglement molecular weight of PS (ca. 13 kg/mol).

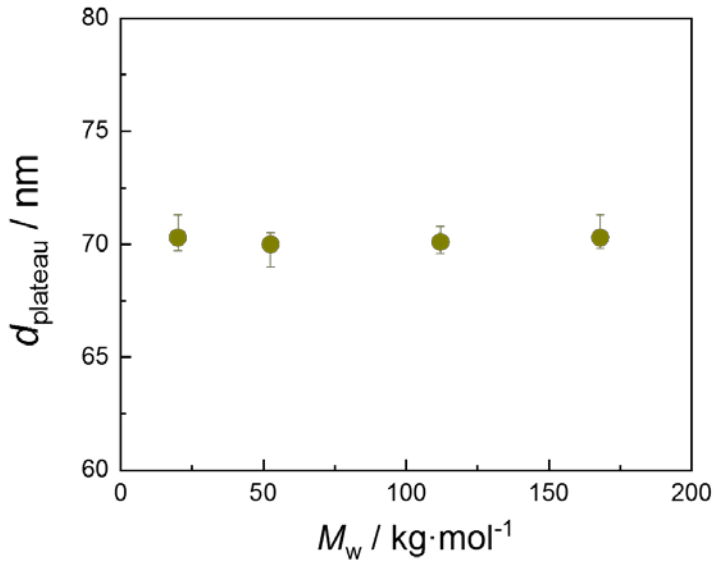


Fig. S7. Invariant height of wetting ridge at plateau region (d_{plateau}) with molecular weight of PS (T = 393 K). This further confirms the formation of wetting ridge plateau region due to rubbery plateau of PS, thus the relation: $d_{\text{plateau}} \sim D_R$. The rubbery compliance of PS is invariant with the chain length, so does the d_{plateau} .

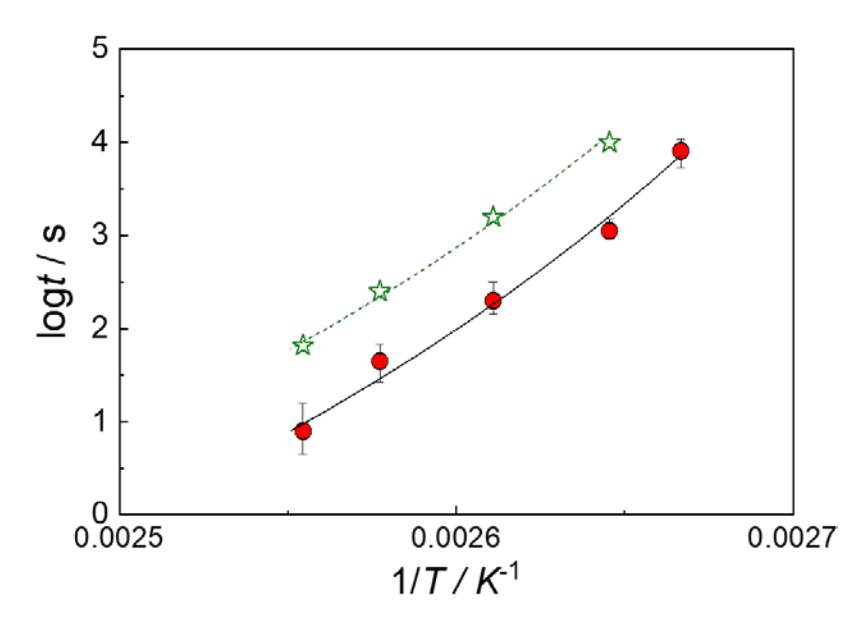


Fig. S8. Comparison of reptation times determined by torsional shear experiments and our nano-creep experiments. Red circles indicate the reptation time from wetting ridge deformation; hollow stars represent the reptation time constant deduced from zero shear viscosity and steady-state compliance obtained by torsional shear experiments in *J. Polym. Sci: A-2. Polym. Phys.* 1971, 9, 209-243. The values of the relaxation times are within an order of magnitude within each other. We believe that the difference is a reflection of the different measurement types and identification of the relaxation times. Importantly, the temperature dependence of the reptation times is the same from both the torsional shear experiments (literature data) and those from the wetting ridge deformation experiments, thus reflecting the same dynamics probed by the two experimental approaches.

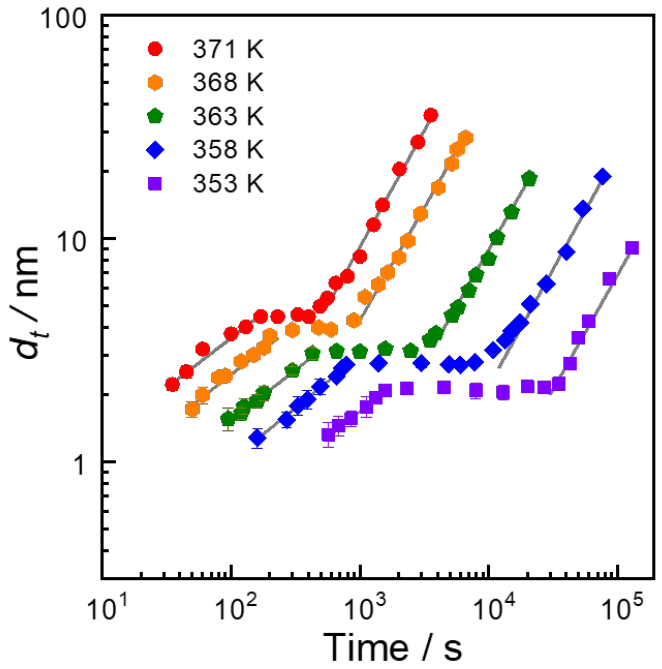


Fig. S9. Time evolution of the d_t at $T_{\rm g,bulk} > T > T_{\rm g,surf}$ (surface dynamics). The $d_{\rm plateau}$ values decrease with decreasing temperature. This can be attributable to the decrement of the size of mobile surface region with cooling and is consistent with the simulation and theory findings. However, the variations in $d_{\rm plateau}$ do not interfere with the determination of relaxation times at various temperatures.

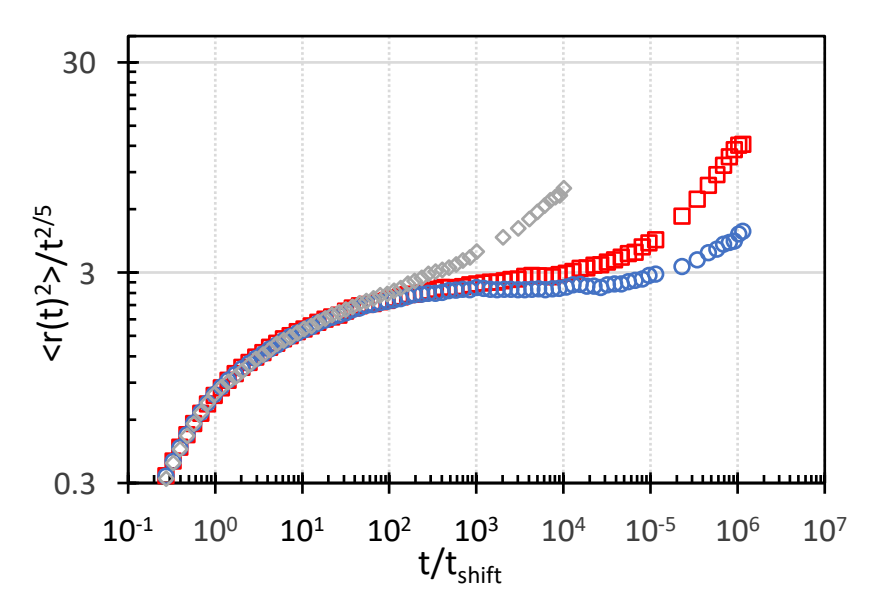


Fig. S10. Mean square displacement over $t^{2/5}$ for simulations of *bulk* systems comprised of 48-bead (grey diamonds), 192-bead (red squares) and 288-bead (blue circles) chains, plotted vs time, at a reduced temperature of 1.60. As seen here, chains with molecular weight of the 192-bead-spring polymer that we employ as a model entangled chain in the main text exhibit an entanglement plateau empirically obeying the scaling $\langle r^2(t) \rangle \sim t^{2/5}$.

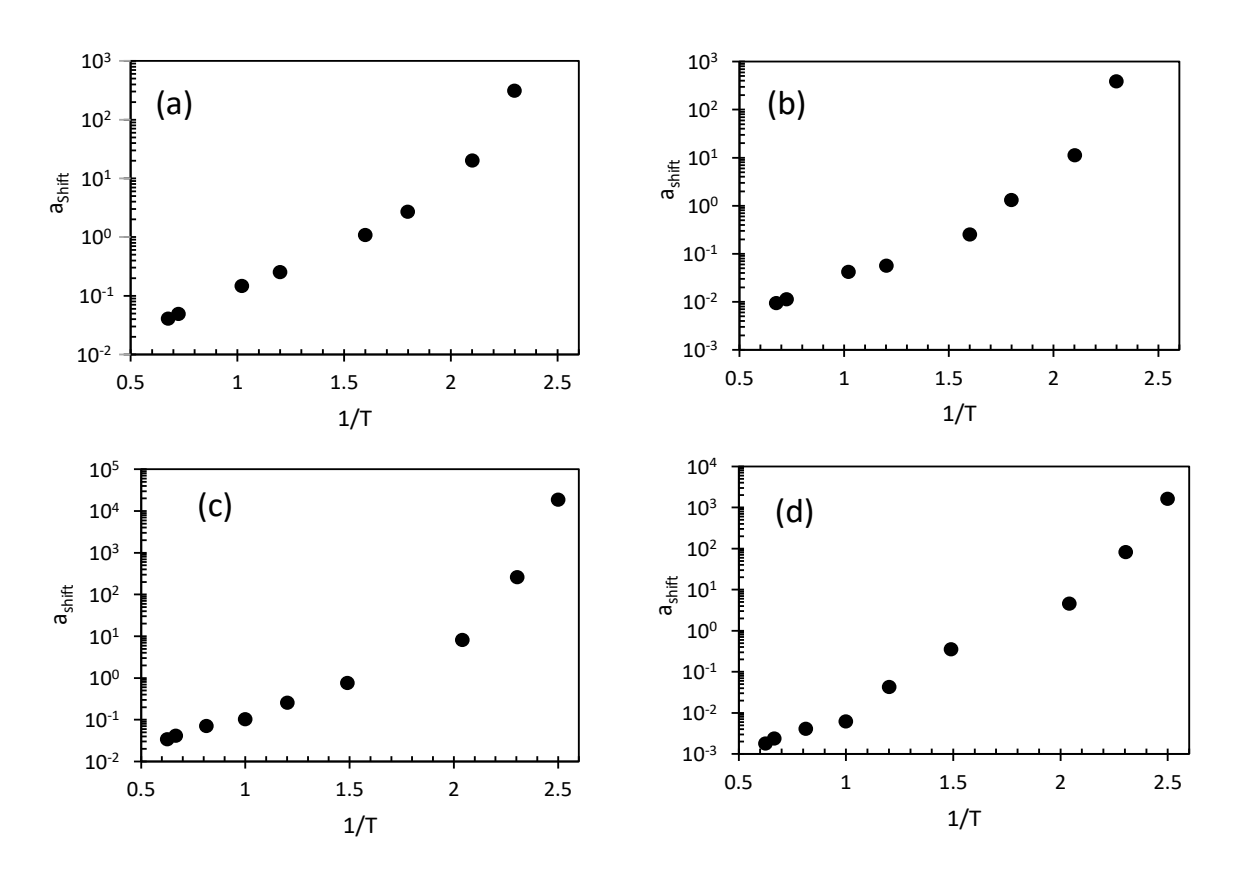


Fig. S11. Plot of *x*-axis (time- axis) shift parameter from simulation, in Lennard-Jones time units, vs inverse temperature, for (a) the 192-bead chain in the midfilm, (b) the 192-bead chain at the surface, (c) the 48-bead chain in the mid-film, and (d) 48-bead chain at the surface.

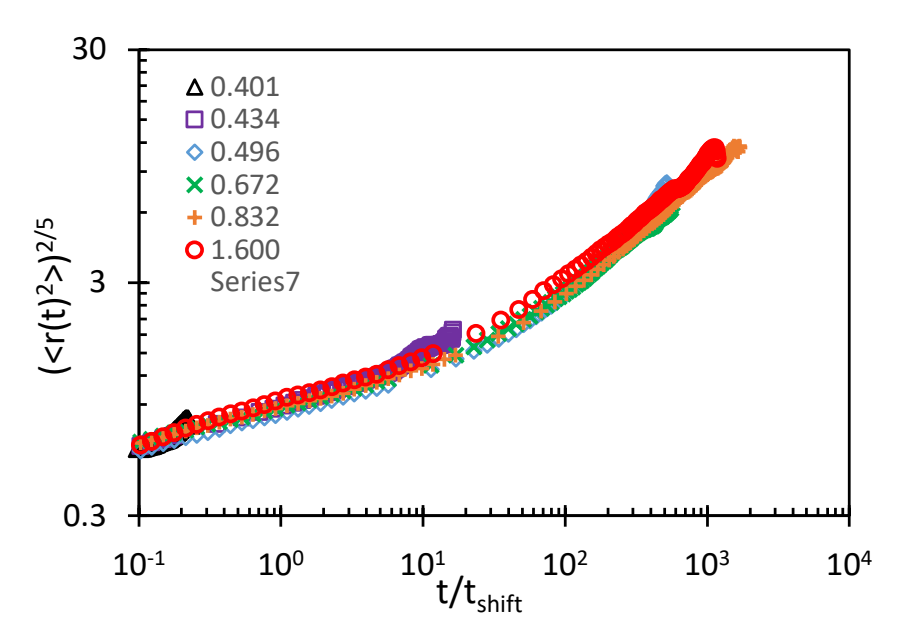


Fig. S12. Mean square displacement over $t^{2/5}$ for simulations of *mid-film* region of simulated films comprised of 48-bead chains, plotted vs time at the temperatures noted in the legend. The data collapse to a single master curve employing shift factors of t_{shift} and $t_{\text{shift}} < r_{\text{shift}} < r_{\text{s$

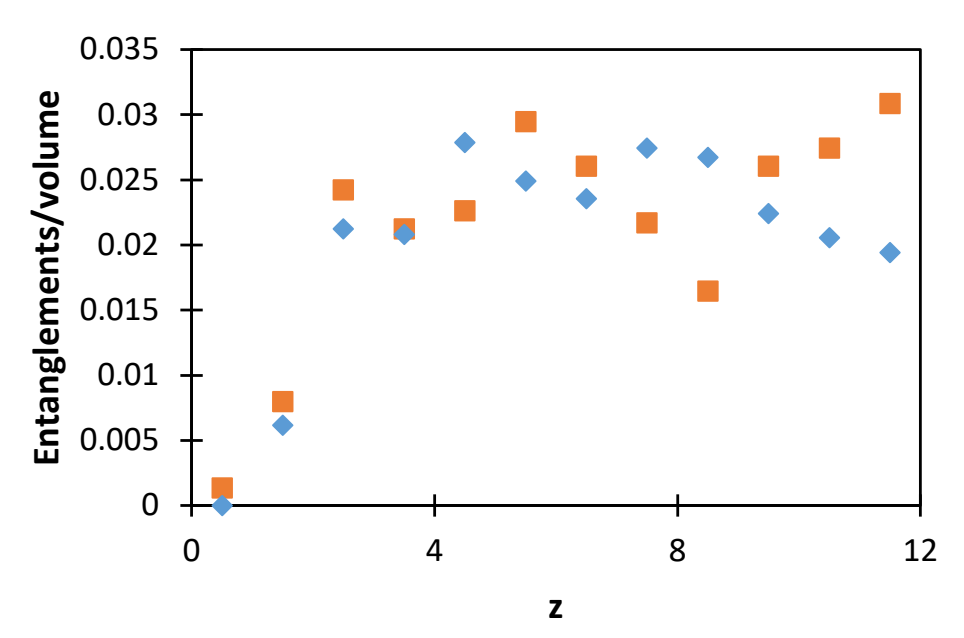


Fig. S13. Number of entanglements per volume as a function of depth in the film for 48-bead chain (orange squares) and 192-bead chain (blue circles), as computed via the Z1 algorithm²⁴,²⁵. Results are at the lowest reduced LJ temperature for each system: 0.402 for the 48-bead chain and 0.435 for the 192-bead chain. Results illustrate a depletion of entanglements (rather than an enhancement) at the film surface, such that topological entanglement cannot drive the interfacial transient elastomeric effect reported in the main text. As shown in the next figure, although the spatial density of topological entanglements is consistent between these two chain lengths (as expected), the shorter nature of the 48-bead chains renders them too short to form an entangled network due to insufficient number of entanglements per chain (the key order parameter for network formation via entanglement).

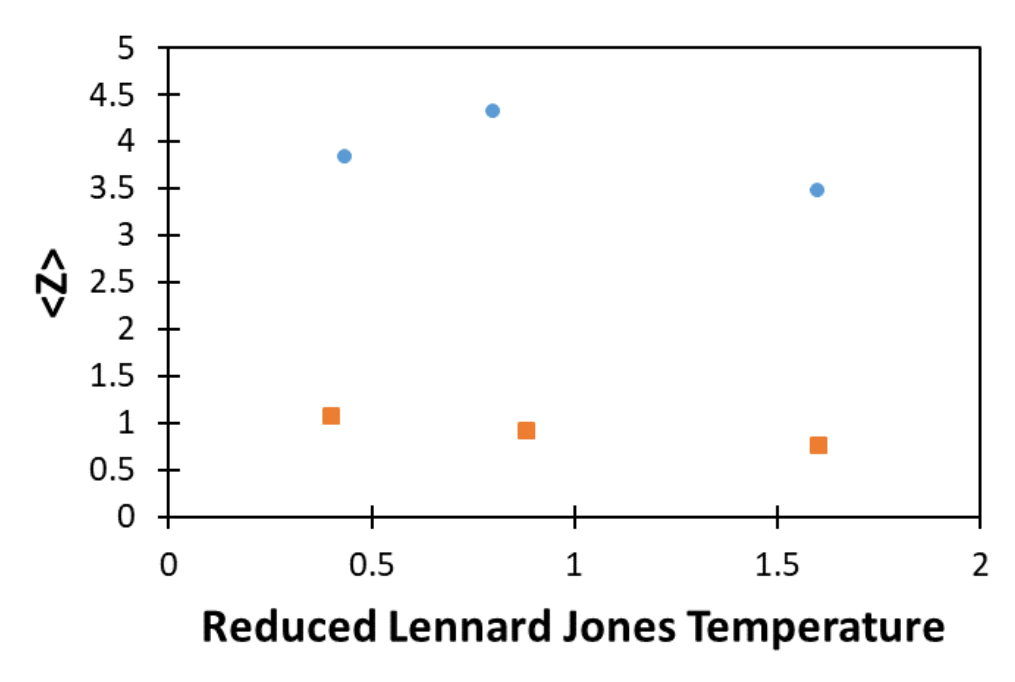


Fig. S14. Average number of entanglements per chain vs temperature for the 192-bead chains (blue circles) and the 48-bead chains (orange squares). The lack of an appreciable growth in these values on cooling provides further evidence that topological entanglements are not the origin of the interfacial transient elastomeric effect reported in the main text. The roughly 4:1 entanglements per chain between the 192-mer and 48 mer chain is consistent with their 4-fold chain length distance and the consistent volumetric entanglement density shown in Fig. S13. The observation of fewer than two entanglements per chain (the percolation transition for crosslinking) in the 48-bead-chain system indicates that it is topologically unentangled, whereas the value of ~4 in the 192-bead-chain system indicates significant topological entanglement.

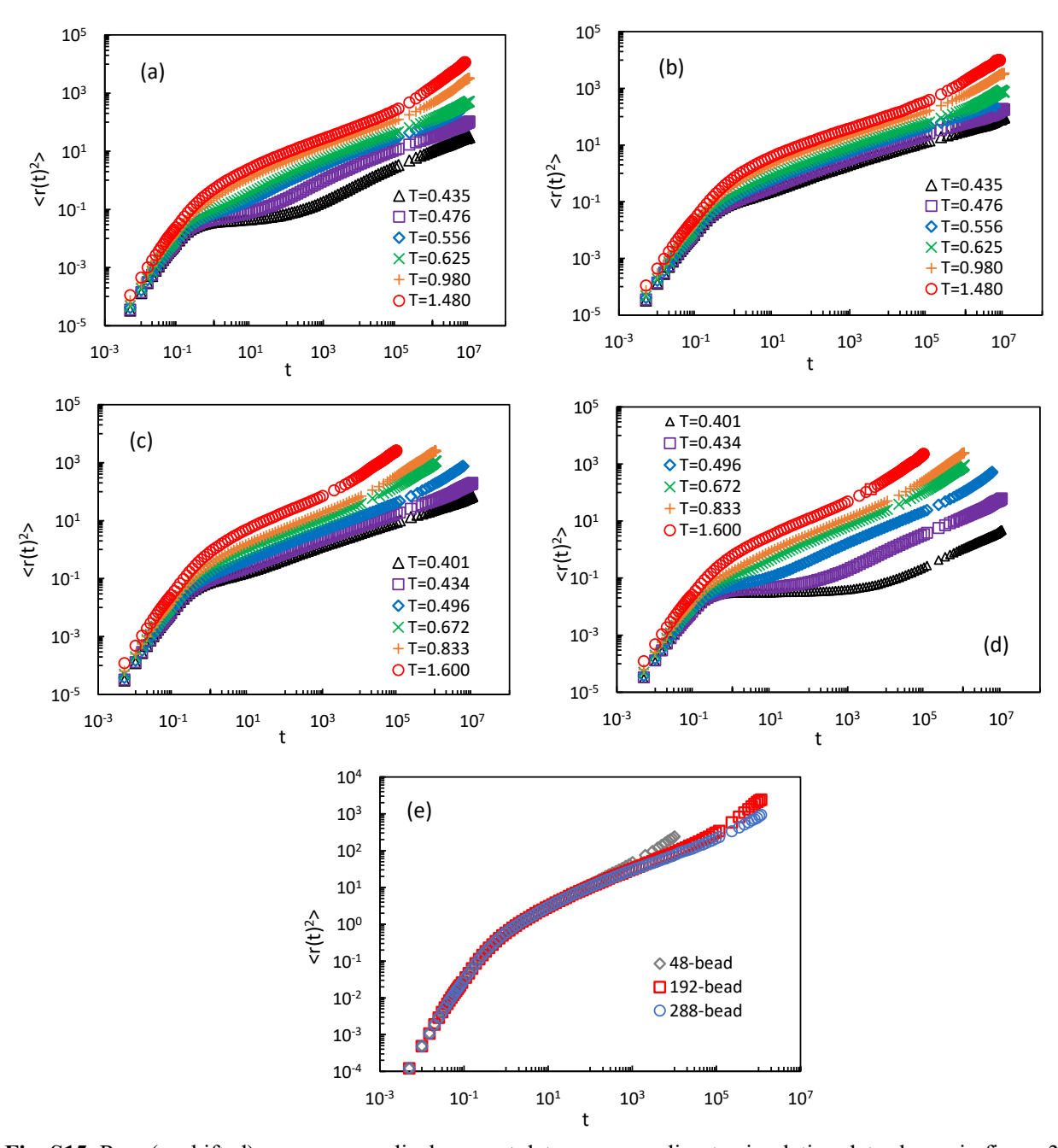


Fig. S15. Raw (unshifted) mean square displacement data corresponding to simulation data shown in figure 3c (a), figure 3d (b), figure 4 (c), figure S10 (d), and figure S12 (e)

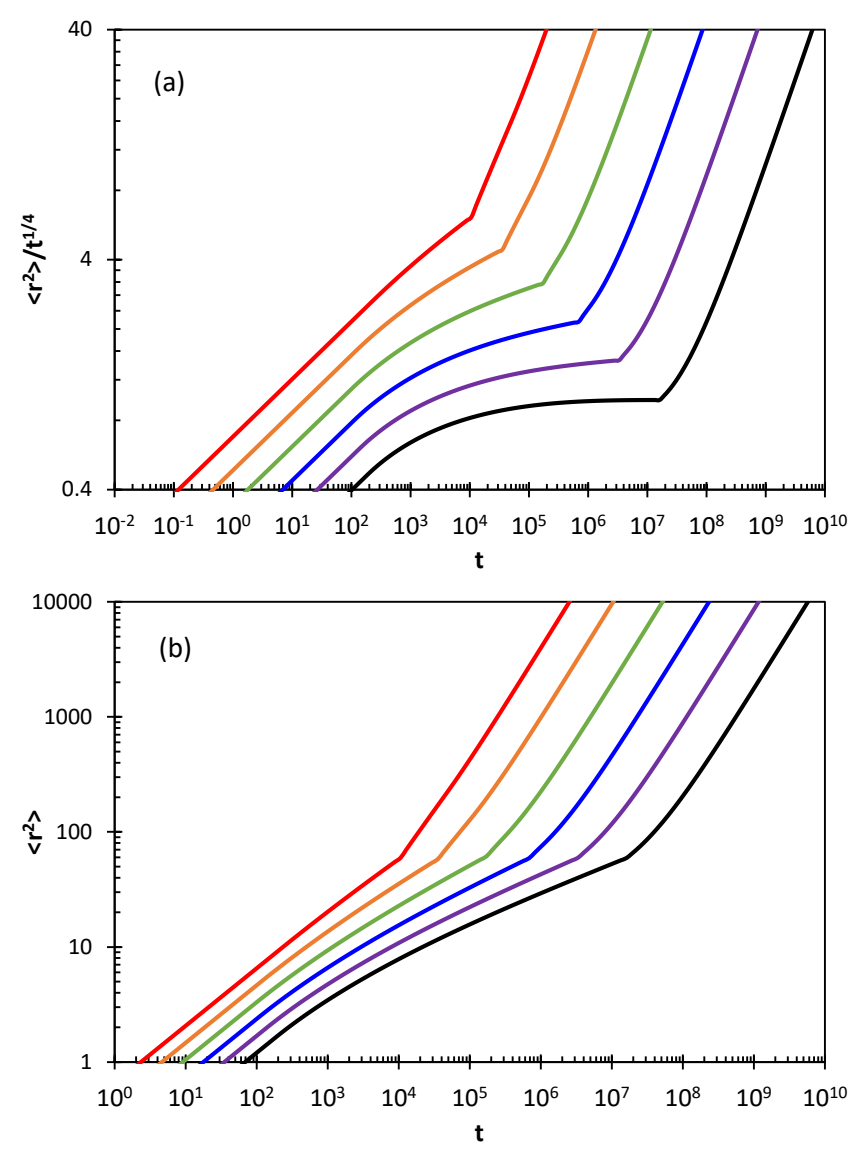


Fig. S16. Raw (unshifted) theoretical predictions of (a) normalized mean square displacement $\langle r^2 \rangle / t^{1/4}$ and (b) non-normalized mean square displacement vs time, for conditions corresponding to the data sets shown in figure 4b. From left to right, curves correspond to bulk relaxation times of 10^0 , 10^1 , 10^2 , 10^3 , 10^4 , and 10^5 Lennard Jones timesteps.

Supplementary References

^{1.} K. S. Schweizer, D. S. Simmons, Progress towards a phenomenological picture and theoretical understanding of glassy dynamics and vitrification near interfaces and under nanoconfinement. *J. Chem. Phys.* **151**, 240901 (2019).

^{2.} J. Baschnagel, F. Varnik, Computer simulations of supercooled polymer melts in the bulk and in confined geometry. *J. Phys.: Condens. Mat.* 17, R851-R953 (2005).

- 3. S. Peter, H. Meyer, J. Baschnagel, Thickness-dependent reduction of the glass-transition temperature in thin polymer films with a free surface. *J. Polym. Sci.: B-Polym. Phys.* **44**, 2951-2967 (2006).
- 4. P. Scheidler, W. Kob, K. Binder, Cooperative motion and growing length scales in supercooled confined liquids. *Europhys. Lett.* **59**, 701-707 (2002).
- 5. P. Scheidler, W. Kob, K. Binder, The relaxation dynamics of a confined glassy simple liquid. *Eur. Phys. J. E* **12**, 5-9 (2003).
- 6. P. Scheidler, W. Kob, K. Binder, The relaxation dynamics of a supercooled liquid confined by rough walls. *J. Phys. Chem. B* **108**, 6673-6686 (2004).
- 7. W. Kob, S. Roldán-Vargas, L. Berthier, Non-monotonic temperature evolution of dynamic correlations in glass-forming liquids. *Nature Physics* **8**, 164-167 (2012).
- 8. G. M. Hocky, L. Berthier, W. Kob, D. R. Reichman, Crossovers in the dynamics of supercooled liquids probed by an amorphous wall. *Phys. Rev. E* **89**, 052311 (2014).
- 9. W. Kob, D. Coslovich, Nonlinear dynamic response of glass-forming liquids to random pinning. *Phys. Rev. E* **90**, 052305 (2014).
- 10. D. Diaz-Vela, J.-H. Hung, D. S. Simmons, Temperature-independent rescaling of the local activation barrier drives free surface nanoconfinement effects on segmental-scale translational dynamics near Tg. *ACS Macro Lett.* **7**, 1295-1301 (2018).
- 11. D. Vela, A. Ghanekarade, D. S. Simmons, Probing the metrology and chemistry dependences of the onset condition of strong 'nanoconfinement' effects on dynamics. *Macromolecules* **53**, 4158-4171 (2020).
- 12. M. Khantha, V. Balakrishnan, First passage time distributions for finite one-dimensional random walks. *Pramana* **21**, 111-122 (1983).
- 13. K. Kremer, G. S. Grest, Molecular dynamics (MD) simulations for polymers. *J. Phys. Condens. Mat.* **2**, SA295-SA298 (1990).
- 14. D. Diaz-Vela, J.-H. Hung, D. S. Simmons, Temperature-independent rescaling of the local activation barrier drives free surface nanoconfinement effects on segmental-scale translational dynamics near Tg. *ACS Macro Lett.* **7**, 1295-1301 (2018).
- 15. D. Vela, A. Ghanekarade, D. S. Simmons, Probing the metrology and chemistry dependences of the onset condition of strong "nanoconfinement" effects on dynamics. *Macromolecules*. **53**, 4158-4171 (2020).
- 16. J. Baschnagel, F. Varnik. Computer simulations of supercooled polymer melts in the bulk and in confined geometry. *J. Phys.: Condens. Mat.* **17**, R851-953 (2005).
- 17. P. Z. Hanakata, J. F. Douglas, F. W. Starr. Interfacial mobility scale determines the scale of collective motion and relaxation rate in polymer films. *Nat. Commun.* **5**, 4163 (2014).
- 18. J-H. Hung, T. K. Patra, V. Meenakshisundaram, J. H. Mangalara, D. S. Simmons. Universal localization transition accompanying glass formation: insights from efficient molecular dynamics simulations of diverse supercooled liquids. *Soft Matter* **15**, 1223-1242 (2018).
- 19. S. Plimpton. Fast parallel algorithms for short-range molecular dynamics. *J. Comp. Phys.* **117**, 1-19 (1995). 20. G. S. Grest, Communication: Polymer entanglement dynamics: Role of attractive interactions. *J. Chem. Phys.* **145**, 141101 (2016).
- 21. D. Ruan, D. S. Simmons, Roles of chain stiffness and segmental rattling in ionomer glass formation. *J. Polym. Sci. B: Polym. Phys.* **53**, 1458-1469 (2015).
- 22. P. C. Hiemenz, T. P. Lodge. Polymer Chemistry. 2nd ed. Boca Raton, FL: CRC Press, 2007.
- 23. K. Kremer, G. S. Grest, Dynamics of entangled linear polymer melts: A molecular dynamics simulation. *J. Chem. Phys.* **92**, 5057-5086 (1990).

- 24. M. Kröger, Shortest multiple disconnected path for the analysis of entanglements in two- and three-dimensional polymeric systems. *Comput. Phys. Commun.* **168**, 209-232 (2005).
- 25. N. C. Karayiannis, M. Kröger, Combined molecular algorithms for the generation, equilibration and topological analysis of entangled polymers: methodology and performance. *Int. J. Mol. Sci.* **10**, 5054-5089 (2009).